Improving veterinary oncology through advanced photon therapy

Diplomarbeit

zur Erlangung des akademischen Grades

Diplom-Ingenieur

im Rahmen des Studiums

Biomedical Engineering

vorgelegt von

David Steinberger

Matrikelnummer 11916471

Ausgeführt an der Technischen Universität Wien

In Zusammenarbeit mit der Medizinischen Universität Wien

Und der Veterinärmedizinischen Universität Wien

Betreuer:

Univ.-Prof. Dr. DI Dietmar Georg,

Wien, 28.07.2022 _____ _____

Unterschrift Verfasser Unterschrift Betreuer

Acknowledgements

I would like to thank Univ.-Prof. Dr. DI Dietmar Georg for giving me the opportunity to work in the Radiation oncology department of the Medical University of Vienna and Vienna General Hospital (AKH Wien) as well as for supervising my thesis. Furthermore, I would like to express my gratitude to Univ.-Prof. Dr. Miriam Kleiter and DI Wolfgang Lechner, PhD for their support and guidance throughout the entire time I worked on this thesis.

I would like to thank my amazing family. Thank you for encouragement, support and love. Without you I would have never come so far.

Finally, I would like to express my gratitude to my friends, especially Matthäus and Tia.

Abstract

Objective:

The advantages of volumetric modulated arc therapy (VMAT) compared to conventional 3-dimensional radiotherapy (3D-RT) with respect to target coverage, sparing of organs at risk (OAR) and plan verification were evaluated for 11 dogs with sinonasal tumors.

Methods:

CT-data of 11 dogs with sinonasal tumors treated with 3D-RT were re-planned with the VMAT technique with the planning system "RayStation 11A". The VMAT and 3D-RT plans were evaluated concerning their dose distribution to the treatment target, and exposure of nine OARs for each patient. Dosimetric limits for each OAR were calculated and each VMAT treatment plan was verified in a phantom on the Linac of the Medical University of Vienna and Vienna General Hospital (AKH Wien).

Results:

The target was irradiated with the same coverage of dose for both 3D-RT and VMAT plans. Compared to 3D-RT, the brain, both eyes and lenses, lower jaw, tongue and ipsilateral lacrimal gland received lower dose, with the VMAT treatment technique. The highest improvements with VMAT were observed in the tongue and lower jaw. Only the contralateral lacrimal gland was spared more effectively in 3D-RT.

Conclusions:

VMAT plans produced the same target coverage as 3D-RT as well as dose conformity. Also, VMAT is a valuable technique for treatment of sinonasal tumors in dogs. Doses to OARs could be reduced with a high delivery accuracy. Low radiation dose to normal tissues should be considered in VMAT.

Kurzzusammenfassung

Zielsetzung:

In dieser Arbeit wurden die Vorteile der Volumetric Arc Therapy (VMAT) im Vergleich zur konventionellen 3-dimensionalen Strahlentherapie (3D-RT) in Bezug auf Zielabdeckung, Schonung von Risikoorganen (OAR) und Planverifikation von 11 Hunden mit Sinonasaltumoren untersucht.

Methoden:

CT-Daten von elf Hunden mit Sinonasaltumoren, die mit 3D-RT behandelt wurden, wurden mit der VMAT-Technik mit dem Planungssystem „RayStation 11A“ neu geplant. Die VMAT- und 3D-RT-Pläne wurden im Hinblick auf die Konformität der Dosisverteilung mit dem Behandlungsvolumen und der Dosisbelastung für neun OARs für jeden Patienten bewertet. Dosimetrische Grenzwerte für jeden OAR wurden berechnet und jeder VMAT-Behandlungsplan wurde in einem Phantom auf einem Linearbeschleuniger der Medizinischen Universität Wien und dem Allgemeinen Krankenhaus der Stadt Wien überprüft.

Ergebnisse:

Die Zielgebietsabdeckung wurde sowohl bei der 3D-RT als auch bei der VMAT-Behandlung mit der gleichen Dosisgenauigkeit bestrahlt. Im Vergleich zur 3D-RT erhielten das Gehirn, beide Augen und Linsen, der Unterkiefer, die Zunge und die ipsilaterale Tränendrüse mit der VMAT-Behandlungstechnik eine geringere Dosis. Die größten Verbesserungen mit VMAT wurden bei der Zunge und dem Unterkiefer beobachtet. Nur die kontralaterale Tränendrüse wurde bei der 3D-RT effektiver geschont.

Schlussfolgerungen:

Die VMAT-Pläne erbrachten die gleiche Zielabdeckung wie die 3D-RT und die gleiche Dosiskonformität. VMAT ist eine wertvolle Technik für die Behandlung von Sinonasaltumoren bei Hunden. Die Dosis für OARs wurde reduziert mit einer gleichzeitig hohen Applikationsgenauigkeit. Jedoch sollte bei VMAT auf eine niedrige Strahlendosis für normales Gewebe geachtet werden.

Contents

List of Figures

List of Tables

List of Abbreviations

CT	Computertomography
FEDIAF	The European Pet Food Industry
IV	Intravenous Therapy
RT	Radiation Therapy
MeV	Megaelectronvolt
Gy	Gray
DNA	Deoxyribonucleic Acid
SSB	Single Strand Breaks
DSB	Double Strand Breaks
NHEJ	Non-Homologous End Joining
HR	Homologous Recombination
LQ	Linear-Quadratic
SF	Surviving Fraction
RF	Radiofrequency
MHz	Megahertz
MV	Megavolt
MLC	Multileaf Collimator
MU	Monitor Units
HU	Hounsfield Units
EPL	Equivalent Path Length
BPL	Batho Power Law
MB	Modified Batho's
CF	Correction Factor

TMR	Tissue Maximum Ratio
EqTAR	Equivalent Tissue-Air Ratio
TAR	Tissue-Air-Ratio
MC	Monte Carlo
GTV	Gross Tumor Volume
CTV	Clinical Target Volume
PTV	Planning Target Volume
OAR	Organ at Risk
DVH	Dose-Volume Histogram
2D	Two-Dimensional
3D	Three-Dimensional
IMRT	Intensity Modulated Radiation Therapy
VMAT	Volumetric Modulated Arc Therapy
AKH	Allgemeines Krankenhaus Wien, General Hospital Vienna
AB	Aktiebolag
EQD2	Equivalent Dose in 2 Gy Fractions
D	Dose
d	Dose per fraction
deg	Degree
min	Minutes
DD	Dose difference
DTA	Distance to agreement
GPR	Gamma pass rate
UZH	University of Zurich

1 Introduction

Similarly, to humans, tumors in dogs occur when mutated cells undergo uncontrolled proliferation instead of following the natural cycle that ends in cell death. Those mutated cells can spread across organs and tissue or metastasize in remote body parts and are defined as cancer [1].

Treatment options for cancer advanced over time and include surgery, chemotherapy and radiation therapy, often used in combination. Radiation oncology has made significant progress due to multiple factors. Due to increasingly sophisticated imaging techniques, the accuracy of target volume definition and delineation was improved. Also, advances in treatment planning systems and linear accelerator delivery capabilities that allow a precise irradiation of the tumor and protection of radiation-sensitive organs and healthy tissue were established. There are two general delivery techniques of radiation therapy; brachytherapy and teletherapy. In brachytherapy, the radiation source is placed near or in contact with a tumor. Conversely, teletherapy is done with the radiation source at a distance from the patient or tumor. These developments are largely driven by the need to reduce the dose to normal tissue structures, thereby minimizing the risk of toxicity and morbidity. This allows the dose to be increased to the tumor volume, potentially improving locoregional control [2], [3].

Those improvements are not only beneficial for humans. As cancer is one of the leading causes of death in dogs, cancer in animals has been studied intensely over the last few decades with significant improvements in medical oncology [4].

1.1 Cancer in Dogs

Spontaneous occurring cancers in dogs affect the animal's health and can be life-threatening. The characteristics of canine dog neoplasia have many parallels to that of their human counterparts, as the biology and heterogeneity of the disease as well as interactions between the immune system and tumor cells are often comparable. Also, dogs can develop different types of tumors on different body locations [4].

1.1.1 Epidemiology

According to a statistic provided by FEDIAF, in the year 2020 around 827,000 pet dogs lived in Austria, excluding strays. Statistically, one in three domestic dogs develops cancer, and around one in two animals above the age of 10 dies from the disease [1], [4], [5].

A statistic from the 1960s shown in Figure 1 stated the most commonly-diagnosed cancers in dogs, differentiated between male and female dogs:

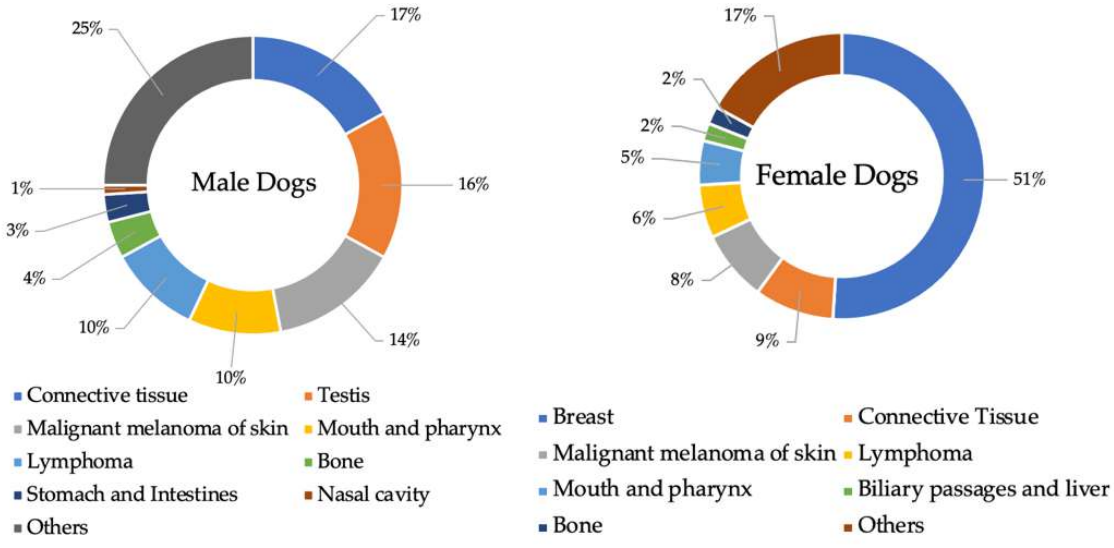

Fig. 1: Estimated numbers of cancer diagnoses (all cancer types) in the 1960s in the USA for males and females at all ages and breed. Source: [6]

While female dogs frequently suffer from mammary cancer and various mesenchymal tumors, male dogs are commonly diagnosed with mesenchymal or testicle neoplasia as well as skin melanomas. This is comparable to humans, as the most common type of cancers for females is also breast cancer. With human males, prostate and skin melanomas are also often diagnosed. [7]

1.1.2 Causes

Any type of cell can transform into a tumor, and it is not always fully understood why this neoplastic transformation occurs. However, some causes have been identified:

Breeding for specific traits and functions leads to a genetic bottleneck in certain dog breeds and are therefore descending from a small number of founder animals. Consequently, some cancer types occur more frequently in certain dog breeds, resulting from a genetic linkage.

Environmental factors can further increase the risk of developing a neoplastic disease. As pet dogs share the same living environment as their owners, they are exposed to the same risk factors. The risk of developing tumors also increases with age - an increase in the average lifespan of dogs has led to an increase in cancer cases in recent decades [4], [6].

1.2 Cancer Treatments for Dogs

The goal of definitive cancer treatment is to fully cure the patient from the disease or to achieve a long-term control.

Unfortunately, some animals suffer from an advanced disease stage that cannot be fully cured or controlled long-term. In this case, the palliative treatment goal is to minimize pain and discomfort and enhance the quality of the animal's life.

A veterinary oncologist has several options for treating pets with cancer, including surgery, chemotherapy, or radiation therapy. Depending on the case, each of these treatments can be used alone or in combination. The overall condition of the dog, as well as their medical history and the tumor type and clinical stage must be taken to account for a final treatment decision [4], [8].

1.2.1 Surgery

Surgery is one of the most important treatment options against tumors in animals. Being the oldest type of therapy, the main goal is to remove as many cancerous cells as possible.

Another treatment intent is to improve the comfort for the pet. When the tumor is hindering normal body functions, removal of a tumor can enhance the quality of life. Further, if the tumor is removed, the damaged neighboring tissue can heal faster.

When the cancer is detected early and has not spread, surgery is the most successful treatment option. Nevertheless, when the tumor location is inaccessible or treatment costs outweigh the benefits, surgery is usually not performed [8].

1.2.2 Chemotherapy

Chemotherapeutic drugs can be administered as a pill, a subcutaneous injection or an IV bolus or infusion. Chemotherapy is given to kill remaining tumor cells.

The dosages required for animals are adjusted according to their body weight or their body surface. A combination of drugs is used in most cases.

Chemotherapy is typically prescribed if the tumor has a high risk of metastasis or if a systemic tumor such as lymphoma is diagnosed.

In an ideal situation, a chemotherapy drug would kill cancer cells in an animal's body without harming normal healthy cells. Whilst chemotherapeutics are highly toxic to tumor cells, healthy cells are also damaged during therapy. This can cause severe temporary adverse effects.

While improvements have been made in chemotherapy for humans, side effects such as nausea, vomiting, hair loss and fatigue are still commonly observed and accepted by oncologists and patients. However, dogs generally appear to be able to tolerate chemotherapy better than humans. Side effects in animals include vomiting, diarrhea, dehydration or inappetence. The most significant side effect is the reduction of white blood cells. Those lower the pet's ability to fight off infections. Hair loss is less common in pets.

Unfortunately, some cancers do not respond to chemotherapy. The response to a drug depends on the cancer type, size, rate of growth and spread and location. As with other cancer treatments, chemotherapy alone usually cannot cure cancer in pets [8].

1.2.3 Radiation Therapy

One of the most common treatments for cancer in both humans and animals is radiation therapy (RT). Cancer cells divide more frequently than normal cells. However, cancer cells also have a weakness: they do not recover from radiation damage as quickly or completely as normal cells. Therefore, radiation works as a treatment for cancer, because it kills cells that divide rapidly and damages them so severely, that they cannot grow further and get destroyed.

The main goal of RT is to deliver just enough radiation to the tumor while minimizing damage to surrounding tissues. For that reason, the radiation is delivered in a series of small doses over several weeks. By administering the radiation in this way, the killing effect on the cancer cells is maximized, while the toxic effects on healthy cells are minimized. This schedule allows healthy cells to repair themselves after radiation exposure.

For brain tumors, nasal tumors and other tumors in the head and neck, radiation therapy may be the treatment of choice. For cancers of the spine or pelvis, it may be the only practical treatment option [8].

Side effects for dogs are divided into acute and chronic subtypes. Acute side effects occur early, tend to be moderate and are usually self-limiting with simple supportive care. They start to develop after the second to third week of treatment on affected tissues like the skin, mucous membranes or the lining of the gastrointestinal tract. Chronic side effects appear gradually over time and take months to years to become evident. Those side effects include scarred vessels and connective tissues with a resulting stiffness, thickening or thinning of tissues as well as a slower healing process when a radiated site is injured [9].

To achieve a high level of accuracy and reproducibility of the RT plans, patients must be immobilized in the correct position during each treatment. Therefore, dogs are put under general anesthesia and positioned in sternal recumbency with head first for the planning CT and daily radiation treatment.

Additionally, vacuum cushions and syringes are in use during CT imaging and RT. As the head is placed on the vacuum cushion, the jaw opening was performed with a $1ml$ syringe. If needed, the syringes were shortened to e.g. $0.4ml$ or $0{,}6ml$ and placed on both fangs on the upper and lower jaw. It gives the possibility to put the patient in an easily reproducible position.

This thesis focuses solely on RT; therefore, it is described in more detail.

1.3 Radiation Physics

The term radiation relates to the emission and propagation of energy through space or a material medium. It can be categorized into electromagnetic radiation and particulate radiation.

Radiation is described by its type and energy. Radiation types fall into two categories: particulate and electromagnetic.

Particle radiation consists of particles with mass and energy, which may or may not have an electric charge. Examples are alpha particles, protons, beta particles and neutrons. Electromagnetic radiation consists of photons, which have energy but no mass or charge. As the quantum theory describes, photons are particles or quanta that contain discrete quantities of electromagnetic energy that travel at the speed of light. Examples of photons are visible light, ultraviolet light, X-rays, and gamma rays.

Furthermore, radiation can be ionizing or non-ionizing, depending on its energy and ability to penetrate matter. Non-ionizing radiation, such as visible light, is harmless. Ionizing radiation is harmful to all tissues, whether malignant or healthy.

Several types of radiation are used for teletherapy: photons, electrons, protons, and heavy ions. Most types of cancer radiotherapy use ionizing high energy photon beams (MV range) for the local or regional treatment of the disease.

As this thesis exclusively addresses photon beams, photon interactions will be discussed in more detail. [10]–[13].

1.3.1 Interaction of Photons with Matter

By passing through medium, an x-ray or gamma ray interacts with the matter, where energy is transferred to the medium. The photon-beam undergoes attenuation, absorption, scattering or transmission. The clinical important interactions

of radiation with matter in RT are the Compton effect, the photoelectric effect and pair production [10].

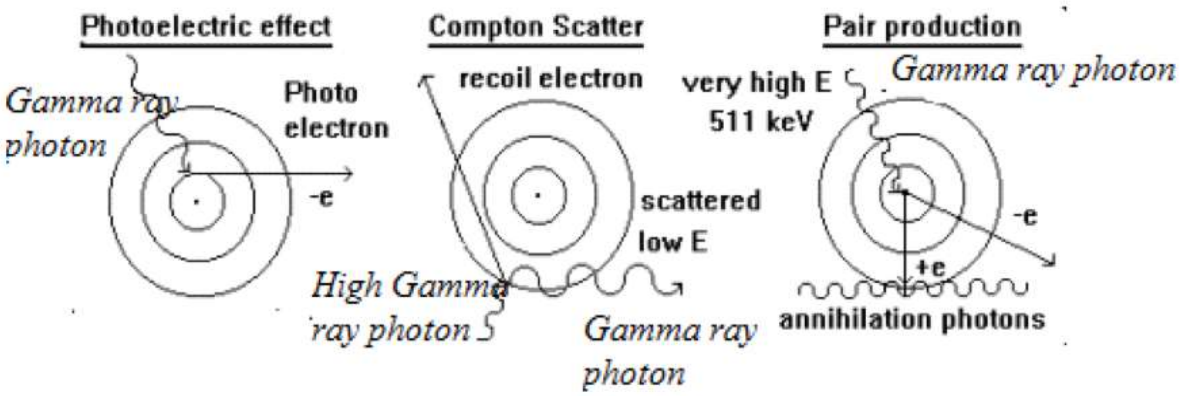

Fig. 2: Photoelectric effect, Compton Scatter, Pair production. Source: [14]

Compton Effect

The Compton effect, shown in Figure 2, has the highest importance in modern-day megavoltage RT. With this effect, photons interact with free electrons and give their parts of their energy to it. As the angle through which the photon is scattered, a relation between the energy handed on the electron and energy lost by the photon can be observed. The wavelength change does not depend on the irradiated material or the radiation energy, only the angle does. Therefore, radiation protection must be designed accordingly [10].

Photoelectric Effect

The Photoelectric effect in Figure 2 shows that the photon transfers all its energy after interacting with the bound electron. The energy is used to remove the electrons from the shell and at the same time is imparted as kinetic energy to the photoelectron. This energy of the characteristic radiation is the fluorescent radiation and differs from atom to atom and for low atomic number elements. Those are most of the biological materials and have very low energy. [10].

Pair Production

Pair production shown in Figure 2 is the result of the interaction with the electromagnetic field of the nucleus. The probability of this process is higher with greater atomic numbers. When a photon with an energy of 1.02 MeV or higher passes close to a nucleus of an atom, the photon disappears and a positron and an electron appear [10].

1.4 Dosimetric Quantities

A photon interacts with a medium in a two-stage-process. In the first stage, secondary charged particles, such as electrons, get their energy from transferred photon radiation, as photons are not capable of a direct deposition of their energy. The energy transfer is done by the photon interactions described above. In the second stage, the electrons transfers energy with atomic ionizations or excitations in the medium. The following two dosimetric quantities describe these two processes [15].

1.4.1 Kerma

Kerma, short for kinetic energy released per unit mass, is a non-stochastic quantity applicable to indirectly ionizing radiations such as photons. It quantifies the average amount of energy transferred from indirectly to directly ionizing radiation.

Hence, kerma is defined as the mean energy transferred from the indirectly ionizing radiation to electrons in the medium $d\bar{E}_{tr}$ per unit mass dm:

$$K = \frac{d\bar{E}_{tr}}{dm}$$

The unit of kerma is Joule per Kilogram $[\frac{J}{kg}]$, whereas the name for the unit is Gray $[Gy]$. $1\ Gy = 1\ \frac{J}{kg}$ [15].

1.4.2 Absorbed Dose

Absorbed dose is also a non-stochastic quantity applicable for both indirectly and directly ionizing radiations. For the indirect, energy is imparted in two steps.

The first step results in kerma, as the indirectly ionized radiation transfers energy as kinetic energy to secondary charged particles. In the second step the charged

particles transfer some of their kinetic energy to the medium in the volume of interest, resulting in absorbed dose and radiative losses.

The absorbed dose is related to the stochastic quantity energy imparted. It is defined as the mean energy $\bar{\varepsilon}$ imparted by ionizing radiation to matter of mass m in a finite volume V.

$$D = \frac{d\bar{\varepsilon}}{dm}$$

The absorbed dose D is given in Gray $[Gy]$ [15].

1.5 Linear Accelerator

Medical linear accelerators, also called medical linacs, are cyclic accelerators that accelerate electrons to kinetic energies, using non-conservative microwave radiofrequency (RF) fields. The kinetic energies have a range from 4 to 25 MeV, the frequency range is from 10^3 MHz (L band) to 10^4 MHz (X band).

High power radiofrequency (RF) fields accelerate electrons. Special devices called magnetrons and klystrons produce the RF fields by decelerating electrons in retarding potentials. Accelerated electrons follow straight trajectories in special evacuated structures called accelerating waveguides. In those waveguides, electrons follow a linear path through the same, relatively low potential difference several times.

For clinical use, different types are in use. Some provide x-rays in the low 4 to 6 megavoltage (MV) range, others provide both x-rays and electrons at various MV energies. Modern high energy linacs provide two photon energies, 6 and 18 MV and several electron energies [16].

1.5.1 Components of modern linacs

A modern linac has five major and distinct sections [16]:

1. Gantry
2. Gantry stand or support
3. Modulator cabinet
4. Patient support assembly (i.e. treatment table)
5. Control console

In Figure 3, a modern medical linac with all its internal connections and relationships between the various components listed above is shown. Figure 3 gives only a general overview. Hence, many variations from different kinds of commercial

machines to others exist. Those depend on the final electron beam kinetic energy and the design of the manufacturer [16].

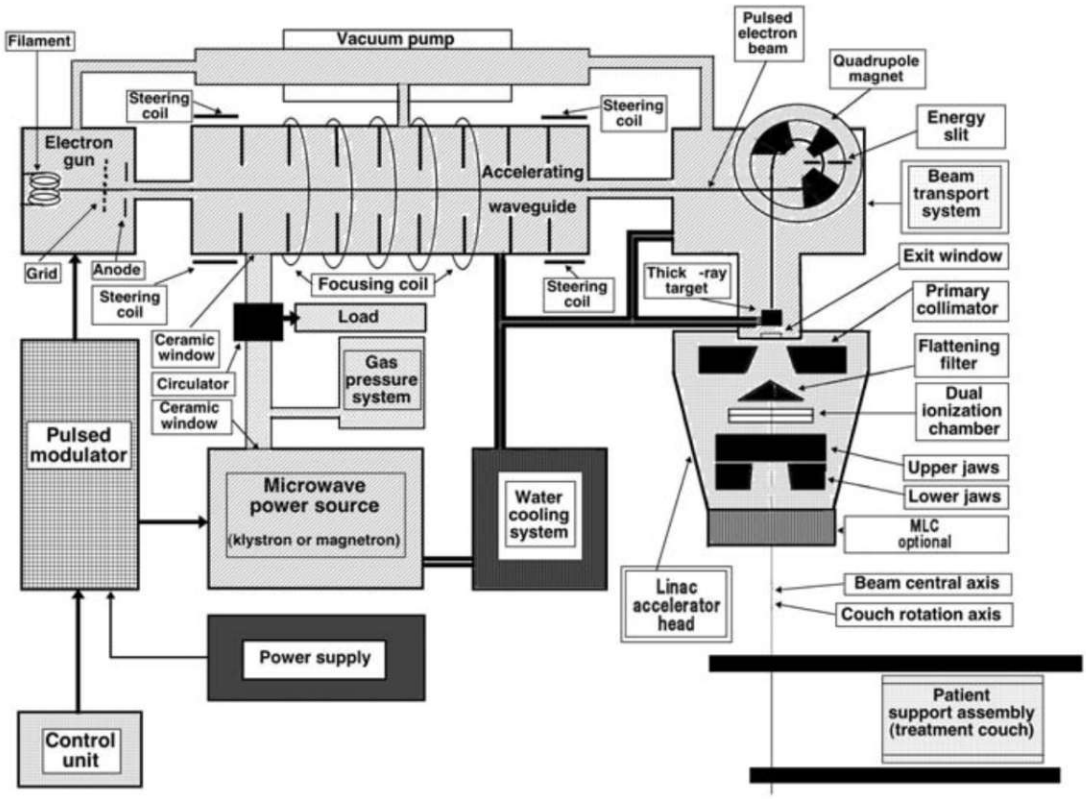

Fig. 3: Medical linac. Source: [16]

Beam forming components are [16]:

1. **Injection system:**

   The source of electrons is an electrostatic accelerator called electron gun.

2. **RF power generation system:**

   The system is used to accelerate electrons to the desired kinetic energy.

3. **Accelerating waveguide:**

   Evacuated or gas filled metallic structures in rectangular or circular cross-section forms, that are used for the transmission of microwaves.

4. **Auxiliary system:**

   This system is not directly involved in electron acceleration but makes acceleration possible due to shielding against leakage radiation, water cooling, air pressure systems and creating a vacuum in the RF generator and acceleration guide.

5. **Beam transport system:**

   Evacuated drift tubes and bending magnets, as well as steering and focusing coils are used for steering and focusing the accelerated electron beam.

6. **Beam collimation and beam monitoring system**

1.5.2 Linac treatment head

The components of a linac head have influence on the production, shaping, localizing and monitoring of the clinical photon and electron beams. The important components in an accelerator head are [16]:

X-ray targets:

X-ray targets produce photon treatment beams. Accelerated electrons and the nuclei of the target material have Coulomb interactions and result in Bremsstrahlung photons. The nucleus decelerates the electron and loses parts of its kinetic energy. The resulting photons have energies ranging from zero to the kinetic energy of the electron. Also, the energy depends on the thickness of the x-ray and the atomic number Z of the target [12], [16].

Flattening filters:

To get a flattened dose distribution, filters are used. They lie between the primary collimator and the monitor chamber. Flattening filters are sources of scattering, leading to a high number of contaminating electrons. Without filters, the dose

rate in the beam is higher and the treatment time is reduced. This is used in intensity modulated RT and stereotactic RT [17].

Beam collimators:

A maximum circular field is defined by the primary collimator. The adjustable rectangular secondary collimator consists of two upper and two lower independent jaws and produces rectangular and square fields at the linac isocenter. Therefore, the moveable secondary collimator shapes the treatment field accordingly to the tumor. Consequently, a higher dose can be delivered precisely to the target volume whilst sparing healthy tissue at the same time. [16].

Multileaf Collimator:

A Multileaf collimator (MLC) is an important tool for modern radiation therapy dose delivery. Originally, the MLC was introduced as a substitute for alloy block field shaping. A MLCs consist of several individual tungsten leaves, that allow to modulate the intensity of the treatment beam as well as beam conforming. The tungsten leaves are remotely controlled and capable to reposition quickly for a different leaf configuration [18]–[20]

Leaf transmission describes how much the treatment beam is attenuated by the height of the leaves, which is controlled by choosing an appropriate thickness (height) of the leaves. However, radiation can leak between the leaf sides of two adjacent leaves or between leaf ends of two opposing leaves, described by the interleaf transmission. To avoid this, interlocking leaves adopt the tongue-and-groove technique seen in Figure 4. An effect of this technique is the possibility of underdosage, as some parts that need radiation could get permanently shielded [21].

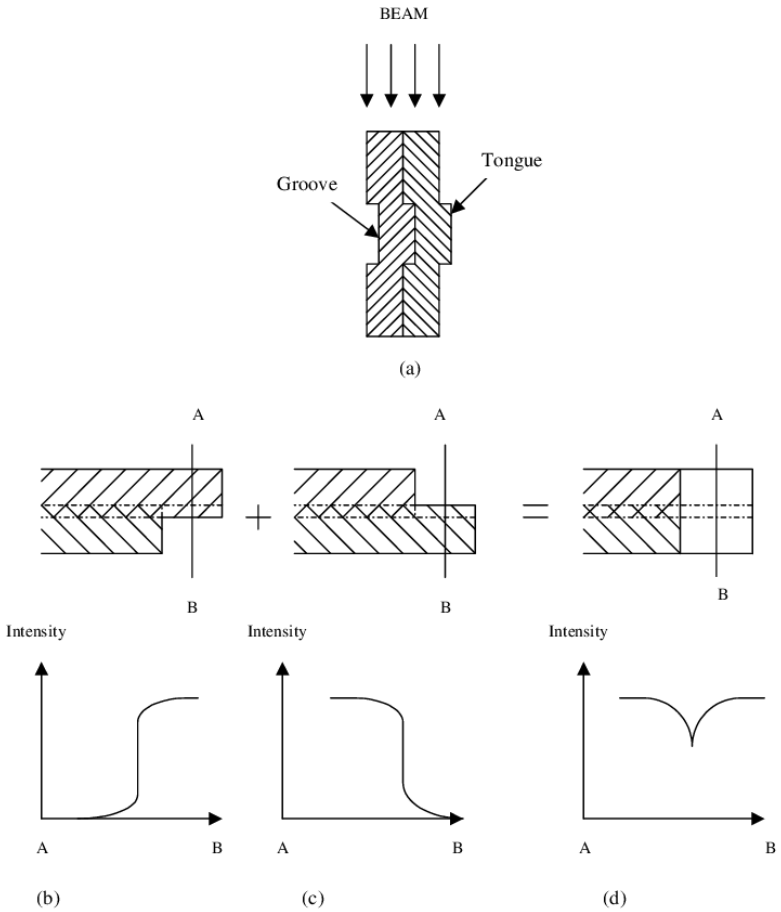

Fig. 4: (a) Design of the MLC tongue and groove to avoid interleaf leakage. (b)-(d) Diagrams of two fields and their superposition defined by two adjacent leaves. (d) Underdosed region of the centered region. Source: [21]

Monitor chambers:

Monitor chambers keeps the flatness, symmetry and uniformity of the beam under control, and are located after the flattening filter in the accelerator head. Additionally, monitor units (MU) are measured by monitor chambers to control if the prescribed dose has been or is delivered properly. For safety reasons, a linac has two monitor chambers, in the case of failure in one [16], [22].

Wedges:

Wedges modulate isodose surfaces, if needed. Physical wedges are made of lead, brass or steel to cause a progressive decrease in the intensity across the beam as well as a tilt of isodose curves. Dynamic wedges provide the wedge effect through a closing motion of a collimator block [16].

1.6 Treatment Planning Systems

As RT linacs have advanced, dose calculation and treatment planning techniques have improved as well. With the invention of computed tomography (CT), three-dimensional dose calculation became possible. Several important advances in RT, i.e. dose distribution, dose optimization, and higher accuracy of patient positioning are attributed to CT. Additionally, the accurate visualization of the geometric location of the patient's tumor and normal tissue is possible due to CTs. The radiation can then be calculated and optimized to determine the optimal dose distribution in the target, avoiding surrounding normal tissue. [3].

The CT image displays the attenuation of the tissue in gray values, the so-called Hounsfield Units (HU). As the HU are related to the attenuation coefficient of the respective tissue, they are converted to electron density and used for the dose calculation [22].

1.6.1 Planning Process

There are two different approaches to carry out a RT treatment plan: forward or inverse planning.

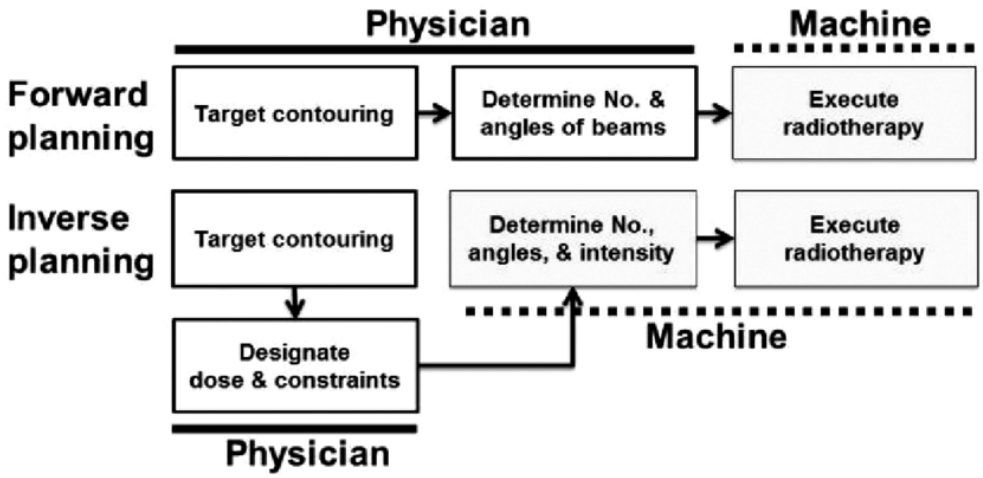

Fig. 5: Forward and inverse planning of a treatment plan in RT. Source: [23]

Forward planning includes three-dimensional conformal RT. With forward planning, parameters like the beam settings, angles of the collimator and wedge as well as the prescribed dose must be determined and entered manually. When a MLC is involved, the shape of the tumor must be conformed for each beam. The configuration of the MLC remains static throughout the treatment session. Hence, the treatment planners' skills are highly responsible for the outcome [16], [24]–[26].

As opposed to forward planning, inverse planning is performed for IMRT and volumetric modulated arc therapy (VMAT) and is based on optimization algorithms. Determination of the treatment technique, the prescribed dose and the number and angles of the beams are necessary and carried out by the planner. Defined treatment volumes, as described in Section 1.6.3, have their dosimetric goals. Therefore, an optimization algorithm tries to calculate the optimal dose distribution iteratively [24], [25].

1.6.2 Dose Calculation Algorithms

In a computerized treatment planning system, dose calculation algorithms are essential. Dose calculation algorithms are used for deriving the correct absolute and relative dose, monitor units (MU) and treatment time.

Generally, two dose types exist [27]:

- Primary dose: A secondary electron is produced by a photon in the tissue. Energy is deposited in the patient's body known as primary dose.
- Scatter dose: Deposited energy of electrons in the patient are created by accelerator head photon scattering. This process adds an absorbed dose, the so-called scatter dose.

Correction based algorithms [27]

Correction based algorithms work with the inhomogeneities of the tissues density information along the beam path from the source to the target given by HUs.

The equivalent path length (EPL) scaling takes the heterogeneities along the fan lines of the beam in one dimension into account. Inhomogeneities across or lateral to the beam direction are not involved in the calculation process. Also, the correction factor is only applied on the primary photon beam kernel, not the scattered photon kernel. This model calculates the change at the depth of dose calculation, due to the presence of a heterogeneity. The density averaged depth at the point of calculation at a physical depth z is given by:

$$z' = \frac{1}{\rho_w}\int_0^z \rho(z'')dz''$$

The density of water is described by ρ_w, $\rho(z'')$ as the density at the local depth (z''), which is calculated from the CT-scan. Therefore, the dose is corrected by replacing the calculated EPL (z').

The Batho power law (BPL) and the Modified Batho's (MB) takes both primary beam attenuation, scatter changes within water and below a single slap of lung material with density relative to water of 0.35 as a correction factor into account.

$$CF = \frac{\left(\mu_{en}/\rho\right)_M}{\left(\mu_{en}/\rho\right)_W}\prod_{m=1}^{N}\left(TMR(z - z_m + z_{bu})\right)^{(\mu_m - \mu_{m-1})/\mu_W}$$

The calculation of the correction factor (CF) is based on the build-up depth-shifted tissue maximum ratio (TMR). μ_m and μ_w are the linear attenuation coefficients of the material in layer m and water. z_{bu} is the build-up depth. z_m is the distance along the beam from the surface to the layer m in the phantom.

Equivalent tissue-air ratio, short EqTAR, corrects the inhomogeneities of the patients' three-dimensional density data. A ray trace is applied to determine the change in the primary dose and to calculate the scatter dose. The tissue-air ratio

depended (TAR) effective depth (ρd) and radius (pr) are scaled according to the relative electron density of the heterogeneous medium.

$$CF = {TAR(\rho d, \rho r)}\Big/{TAR(d, r)}$$

Algorithms based on convolution [27]

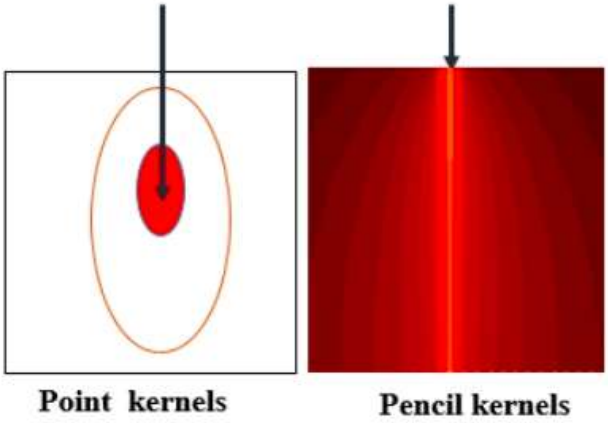

Fig. 6: Irradiation geometries for point kernels and pencil kernels. Source: [27]

Primary photons can travel large distances independent of energy and direction. Energy deposition of secondary particles around a primary photon interacts in way that can be described by a kernel. Kernels are defined as the distribution of energy imparted per unit volume elements in a medium, due to a photon beam interaction at the origin of the coordinates of the kernel. Figure 6 shows the categories of kernels: point kernels and pencil kernels.

A point kernel describes the pattern of energy deposited in an infinite medium around a primary photon interaction. The calculation of dose from point kernels is divided in two steps. First, the released energy in the patient trough attenuation of primary photons is calculated by ray-tracing primary photon trajectories. Secondly, the dose is calculated by superposition of appropriately weighted kernels. To take the heterogeneity into account, a common approach is to scale all

dose fractions of a point kernel $h\rho_0$ and calculate them as a homogeneous medium with a mass density ρ_0. At the point (s) energy is released, at the point (r) energy is deposited. Hence, the dose can be calculated as:

$$D(r) = \iiint_v T(s)\,{}^{\rho(s)}/_{\rho_0}\, c^2 h\rho_0[c(r-s)]d^3s$$

Nevertheless, the point kernel calculations are more time consuming.

A pencil kernel describes the energy deposition in a semi-infinite medium from a point mono-directional beam. As hybrid algorithm, it takes full account for beam modulations and field shapes. They handle heterogeneities and patient characteristics by scaling and correction methods. However, scatter dose calculations in patient sizes are a limitation. The dose is calculated by:

$$D(r) = \iint_s \int_E \iint_\Omega \sum_m \Psi^m_{E,\Omega}(s)\frac{p^m}{\rho}(\curlyvee, \Omega, s, r)d^2\Omega dE\, d^2s$$

The energy fluency differential in energy E and direction Ω for beam modality m is described by $\Psi^m_{E,\Omega}(s)$. $\frac{p^m}{\rho}(E, \Omega, s, r)$ is the corresponding pencil kernel for energy deposition per unit mass at $\curlyvee$ due to primary particles entering the patient at s.

Monte Carlo dose calculation [27]

MC dose calculation is the most accurate algorithm. This simulation-based calculation uses probability distributions and physical principles.

The method uses photon and electron transport compounds to consider the trajectories of individual particles. Their patterns of dose deposition are also taken to account. Each particle is determined by a random number generator individually with millions of tracings generated. The dose distribution is built by summing the energy deposition of each particle, as it models each photon interaction in the patient.

The limitations are given by the fact that is highly time consuming and expensive, as the computational demand is extremely high.

1.6.3 Treatment Volumes

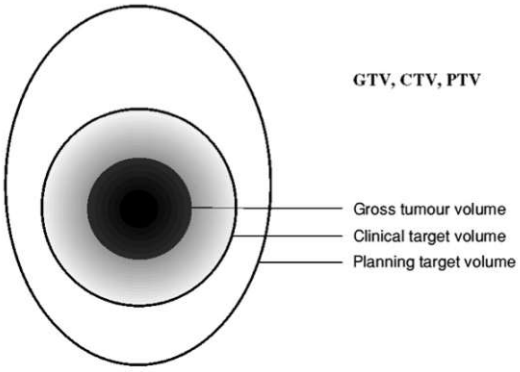

Fig. 7: Illustration of the main RT planning volumes. Source: [28]

As RT is a localized treatment, the definition of tumor and target volumes is essential. Consequently, the best possible characterization of the location and extent of the tumor is required [28].

For this thesis, the four main volumes in RT planning are GTV, CTV, PTV and OAR.

Gross Tumor Volume (GTV)

GTV is the volume that can be seen, palpated or imaged. It is strictly the demonstrable location and extent of the tumor, where the tumor cell density is the highest. Therefore, it strictly follows the boundaries of the seen neoplasm, without adding any possible extension. If lymph nodes are involved, they also should be also included in the GTV [28], [29].

Clinical Target Volume (CTV)

Beyond the GTV, a volume that contains microscopic tumor spread is called the CTV. This spread is too small to be visible for imaging procedures, but it can be the source of treatment failure. Those failures are due to a direct spread around the tumor or drainage of lymphatic vessels and nodes. However, knowledge on microscopic spread is often based on statistics of distant invasion, which is gathered through careful analysis of surgical series. Thus, the choice of irradiating a volume of possible cancer spread or not is based on judgement of appropriateness [28], [29].

Planning Target Volume (PTV)

The PTV encloses the CTV with anisotropic margins to account for possible uncertainties. These involve the beam alignment, positioning of the patient, motion or organs and deformations of organs [30].

Organ at Risk (OAR)

OARs are healthy tissues or organs placed near the PTV, whose irradiation could cause damage. Due to their location, they might receive unplanned doses during RT [31]. When those structures are radiation sensitive, it is important to know their dosimetric limits with respect to radiation toxicity. Hence, it is important to contour them accurately on CT scans [26].

1.6.4 Dose-Volume Histogram

Dose-Volume Histograms (DVH) summarize the dose distribution information over a three-dimensional matrix of points over the patient's anatomy. Used as a tool to evaluate treatment plans, it represents a frequency distribution of dose values within a defined volume. Those volumes could be the PTV, CTV, GTV or

OARs. On the x-axis, the dose in Gy is shown against the volume in per cent on the y-axis.

The first subtype is the direct or differential DVH. The average dose of a given range in each volume is summed up. The resulting percentage of the volume is then plotted. In this case, the ideal direct target DVH would have a narrow single column, showing that a 100% of the volume receives the prescribed dose. The ideal DVH for critical structures, such as the OARs, would have a total dose of 0 Gy over the complete x-axis. As Figure 8 depicts, the peak for the target is not as narrow as always wished. As illustrated in Figure 9, OARs may contain several peaks, indicating that different parts of an organ or tissue receives different doses.

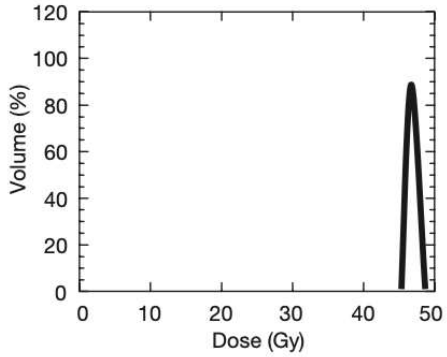

Fig. 8: Example of a direct target DVH. Source: [16]

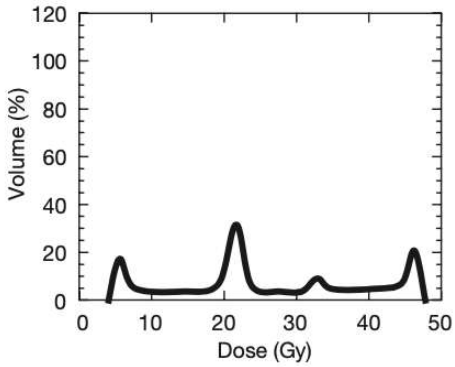

Fig. 9: Example of a direct DVH of an OAR. Source: [16]

The second subtype is the cumulative or integral DVH. This type is used more often for plan evaluations. The plot shows the percentage of a volume, i.e. the PTV and OARs on how much dose those receive. It starts at 0 Gy on the x-axis, as a 100% of the volume gets at least no dose.

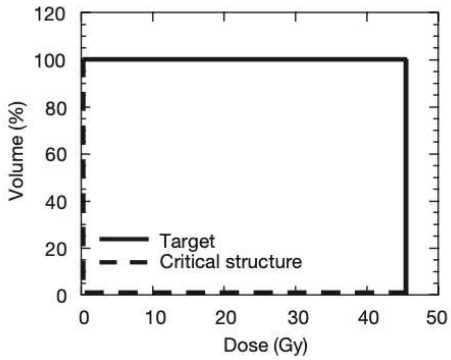

Fig. 10: Example of an ideal cumulative DVH. Source: [16]

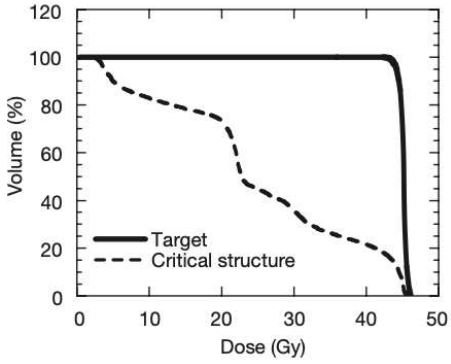

Fig. 11: Example of a realistic cumulative DVH. Source: [16]

Figure 10 depicts an ideal cumulative DVH of a target and an OAR. A constant high percentage, in the best case a 100%, is delivered to the target. At the same time, the OAR is ideally spared completely and does not receive any dose. In practice, this is not possible. In RT, it is always necessary to find a way to irradiate the target with about 95% of the described dose and save the OARs and other critical structures at the same time. This is seen in a more realistic cumulative DVH in Figure 11. Hence, tolerances must be calculated to have a satisfying outcome of the RT without damaging too much of the patient's body [16].

1.6.5 Patient Specific Quality Assurance

Radiation dose escalation can be beneficial for local control and improving overall survival in the treatment of cancer. However, these benefits may be accompanied by higher incidences of acute and late toxicity. To evaluate the desirable target coverage and toxicity reduction to OARs, quality assurance of the treatment planning system and of a respective treatment plan is indispensable.

The gamma index γ is one of the most commonly used metrics for the verification of a complex, modern radiotherapy. The γ index combines dosimetric and geometric aspects, because it requires the specification of dose and distance-to-agreement (DTA) criteria for acceptable variations between two dose distributions. The dose-difference computes the numerical dose difference between the two dose distributions at common points. DTA is computed for each reference dose point and examines the evaluated dose distribution for the nearest location that has the same dose as the reference point. The γ index measures the closest point in one of the dose distributions (the evaluated distribution) with individual points of the other distribution (the reference distribution), when the two distributions are normalized by the dose difference and DTA criteria for the dose and spatial coordinates, respectively. The closest point in the evaluated distribution to a selected reference distribution point is the value of γ at the reference point. Traditionally, γ has been used to compare a 2D measured plane against a 2D or 3D dose distribution. Recently, software algorithm and hardware improvements have led to the possibility of using measured 2D data from commercial detector arrays to reconstruct a 3D-dose distribution and perform a volumetric comparison against the treatment planning system (TPS). Hence, a quality assurance for each treatment plan can be performed [32]–[34].

1.7 Treatment Techniques

After the discovery of RT, a systematic development of the practice occurred. The need to focus the radiation in the tumor whilst sparing normal structures was understood early. Additionally, advances in mathematics, therapy planning techniques, radiation technology and three-dimensional imaging helped to invent modern treatment techniques [35].

1.7.1 Conventional Radiotherapy

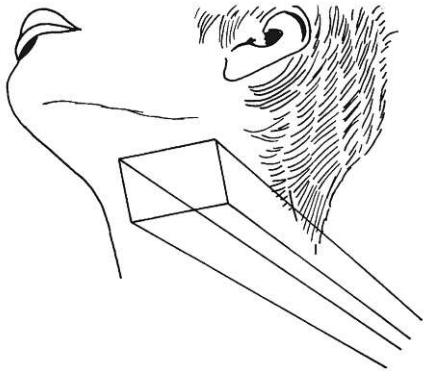

Fig. 12: Illustration of a conventional RT. Source: [35]

Based on 2D X-ray images, one of the first treatment techniques was the now outdated conventional, two-dimensional (2D) RT. It consisted of a single beam that was capable of irradiation in one to four directions. The setups and the shapes of the beams were simple and plans frequently consisted of opposed lateral fields or four-field boxes. This led to negative side effects, as adjacent tissues and organs fell into the high dose region. Therefore, the treatment was less efficient than today's technologies [36].

1.7.2 Three-Dimensional Radiotherapy (3D-RT)

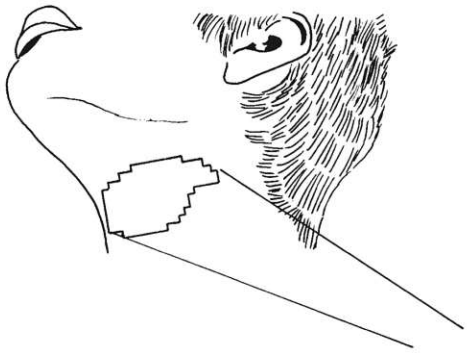

Fig. 13: Illustration of 3D-RT with a MLC in use. Source: [35]

Three-dimensional, or CT-based RT, takes anatomy and complex tissue contours into account. Due to the 3D-CT images, the target as well as the surrounding OARs are locatable and can be therefore contoured precisely [36].

The number of beams and their angles depends on the type of cancer as well on the patient. When a MLC is used, it is possible to shape the beam accordingly to the tumor shape. This configuration remains during dose delivery. Wedges can also be used [37].

As a result, doses next to the tumor are reduced, while the target receives a high dose delivered. However, this treatment technique is limited by its inability to exclude normal tissues surrounded by tumor in its entirety. This is due to the uniform intensity of the beam [37].

1.7.3 Intensity-Modulated Radiation therapy (IMRT)

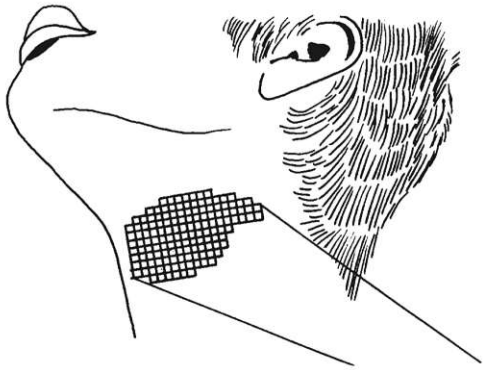

Fig. 14: Illustration of IMRT using intensity modulation. Source: [35]

To overcome the limitations given by 3D-RT, two key additional features are added:

1. Non-uniform intensity of the radiation beams
2. Computerized inverse planning

The intensity of the radiation is variable, each beam is subdivided into hundreds of beamlets with an individual intensity. This allows irradiation of the target in complex patterns that fit the tumor shape and size. When multiple beams are used, the precision of the beam is further improved and thus the surrounding organs and tissues are spared more effectively.

The computerized inverse planning allows to specify the plan outcome in terms of the dose limits of the OARs and the aimed tumor dose. The system adjusts the beam intensity to find the best configuration for the desired outcome to avoid dose escalations and to create an intentional dose inhomogeneity.

Despite the benefits, the planning and quality assurance processes are more complex. The planning time is therefore increased, as the OAR and target outlining is more extensive. Also, the treatment machine time is increased [37].

1.7.4 Volumetric Modulated Arc Therapy (VMAT)

Volumetric modulated arc therapy (VMAT) is a modern form of intensity modulated radiation therapy that achieves precisely shaped 3D dose distribution during rotation of the gantry around the patient. The adjustable parameters during treatment are:

- Dose rate
- Size and shape of the irradiation field
- Rotation speed of the gantry

By using special software and a modern linear accelerator, dose conformity can be improved while treatment times can be significantly reduced (up to eight times) compared to IMRT. Rotational irradiation typically takes less than two minutes. A short treatment time in RT is beneficial. Firstly, organ motion can be reduced. Secondly, patients do not have to lie down for long periods of time, especially while suffering from severe pain.

VMAT, like IMRT, is used for highly irregular volumes. With this advanced irradiation technique, tumors in the immediate vicinity of vital organs can be treated more safely and effectively without damaging them with high radiation doses. For example, in the case of irradiation of the prostate, rectum and gynecological tumors, it is possible to spare the intestine and bladder better. In the case of tumors in the head and neck region, highly sensitive organs and tissues like the spinal cord, salivary glands, optic nerves and brain stem can be spared [2], [38].

1.8 Tumors of the Nasal Cavity and the Paranasal Sinus of the Dog

A tumor in the nasal cavity and the paranasal sinus is an insidiously expanding, space-occupying mass in the sinonasal region of dogs as seen in Figure 15. Adjacent structures can be invaded, destructed and can result in a loss of function.

The largest pooled data set analyzed 504 canine intranasal tumors. In this data set, 88% were diagnosed in the caudal regions of the nasal cavity, 6% in the sinuses and 6% were multicentric [39].

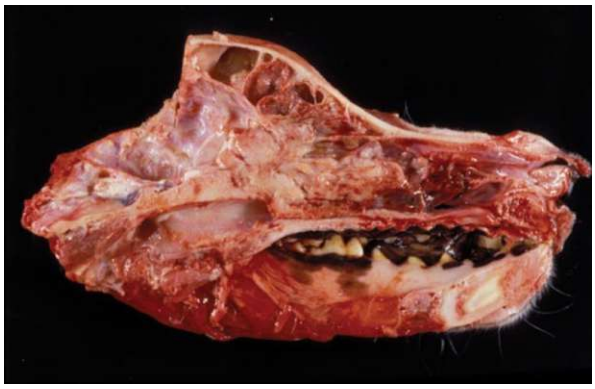

Fig. 15: A mass replaces the turbinates in the caudal nasal cavity. Source: [39]

1.8.1 Prevalence

Only approximations can be stated, as variations in sample populations, sample bias or inconsistencies in diagnoses are influential factors on the data. Population-based incidence reports a rate of 2.5 sinonasal tumors per 100,000 dogs. Data from survey of hospital admissions have been used to calculate rates of 81 per 100,000 dogs at risk or 38 per 100,000 medical admissions. These numbers show that (and as Fig. 1 stated above) tumors of the nasal cavity and paranasal sinuses in dogs present around 1-2% of all neoplasia. Therefore, they are not as common as other tumors in dogs, such as mammary cancer or cancer of the connective tissue [39], [40].

1.8.2 Age, Breeds, Sex

While the mean age of dogs with sinonasal tumors ranges between the age of 8 to 10 years, the greatest risk occurs approximately between the age of 10 to 15 years. Nevertheless, nasal tumors have been observed in dogs of less than 6 months and more than 16 years of age.

Some breeds have a greater risk to develop a sinonasal tumor. In decreasing order, Airedale Terrier, Basset Hound, Old English Sheepdog, Scottish Terrier, Collie and German shorthair pointer are reported to be at a higher risk to develop intranasal cancer. Brachycephalic breeds with short snouts have a decreased risk to develop intranasal tumors, an exception is the Boston Terrier. Hence, it is controversial to state that the snout length has influence on the risk to develop an intranasal neoplasm.

Pooled hospital data report a male-to-female ratio of 1.3 to 1. In some other studies, an overall male predominance was observed. This ratio varied among breeds and tumor type and was not confirmed in several other studies [39], [40].

1.8.3 Tumor Types

Data from major veterinary hospitals showed that of 239 recorded tumors, 82% were malignant and only 18% were benign. A benign tumor grows slowly and has distinct borders, does not invade surrounding tissues or other parts of the body. Malignant tumors can grow quickly and have irregular borders. They typically invade surrounding tissue and can spread to other parts of the body through a process called metastasis. Malignant tumors of the nasal cavity and paranasal sinuses in dogs are slow to metastasize and locally invasive [39]–[41].

The following Tab. 1 shows an excerpt of the classification of sinonasal tumors. The classification divides the tumor in two types. Epithelial malignant tumors are called carcinomas, mesenchymal tumors are called sarcomas [42], [43].

Epithelial Tumors		Mesenchymal Tumors
Benign	Malignant	-
Papilloma	Squamous cell carcinoma Transitional carcinoma Adenocarcinoma Adenoid cystic carcinoma Acinic cell carcinoma …	Fibrosarcoma Chondrosacroma Osteosarcoma Malignant mesenchymoma Lymphoma …

T. 1: Classification of sinonasal tumors. Source: [39]

Around 60% of malignant tumors in the nasal cavity are carcinomas, while the other 40% are of mesenchymal tumors or cancer of other origins. Adenocarcinomas are the most common carcinomas, followed by transitional and squamous cell carcinomas. Chondrosarcoma is the predominant sarcoma subtype, followed by osteosarcoma and fibrosarcoma [39].

1.8.4 Clinical characteristics

Sinonasal tumors grow rather slowly and cause their clinical signs are caused by space occupation, local destruction and invasion. The most frequent clinical sign is unilateral or bilateral nasal discharge, which can be bloodstained. Other signs involve sneezing, facial deformity, ocular discharge, or epistaxis. If the tumor has invaded through the cribriform plate into the brain, neurologic signs can also occur [39], [40].

At diagnosis, most malignant sinonasal tumors do not have detectable metastases. Metastasis can happen later in the course of the disease. An overall metastasis rate of 41% at the time of death has been reported in 120 necropsies. Most of those cases had a local extension into the cranial cavity and the brain. Only 16% of 68

carcinomas had metastases into regional lymphnodes and 12% into the lung. Sarcomas are less likely to metastasize, as only 8% had pulmonary metastases [39].

1.8.5 Diagnosis

Computed tomography (CT) provides a high certainty to establish the tentative diagnose a sinonasal tumor. CT provides information about local tumor extension, bone destruction and detection of abnormal soft tissue density. Definitive diagnosis is confirmed with a biopsy. With a rhinoscopy, rhinotomy or transnostril blind biopsy, tissue samples are obtained. During the process, the distance from the eye to the naris should be measured externally to prevent accidental penetration of the cribriform plate [39], [40].

1.8.6 Staging

Sinonasal tumors are staged according to the modified Adams tumor staging system. Four stages describe the severity of the local tumor extension as well as potential local or distant metastasis. In stage 1, only one nasal passage is involved. There is no bone destruction beyond the turbinates. In stage 2, there is bone involvement, however there is no evidence of an orbital, subcutaneous or submucosal mass. This changes with stage 3, as an orbital nasopharyngeal, subcutaneous or submucosal involvement can be found. When a stage 4 tumor is diagnosed, a tumor-associated lysis of the cribriform plate is observed [44].

1.8.7 Treatment and Prognosis

Although the long-term prognosis for canine sinonasal tumors is poor, radiation therapy has been shown to increase the overall survival time. A study stated that without any treatment, the median survival time was approximately 3 months. With full-course radiation therapy, median survival times was ranging from ap-

proximately 12 to 16 months. After therapy, patients may continue to show clinical signs related to the tumor, although these are usually less severe than before the treatment. This study found that only 39% of dogs were completely free of clinical signs after radiation therapy [40].

1.9 Radiobiology

The goal of RT is to induce cell death to the malignant cells. When a cell has lost its reproductive integrity, they are by definition dead. This is mainly caused by lesions in the deoxyribonucleic acid (DNA), which has all the genetic information in its structure. The specific damages in the DNA caused by radiation are:

- Single strand breaks in the phosphodiester linkage
- Double strand breaks on opposing or displaced sites
- Base damages
- Damages of the protein-DNA
- Protein-protein crosslinks involving nuclear proteins.

The number of lesions in the DNA of a cell by a dose of $1-2\ Gy$ are approximately:

- Base damages > 1000
- Single strand breaks (SSB) ≈ 1000
- Double strand breaks (DSB) ≈ 40

DSBs play a critical role in cell killing. They correlate with radiosensitivity and survival at low dose.

However, there are multiple enzymatic mechanisms of DNA repair in cells that act on different types of lesions. DSB are repaired by two primary pathways, the so-called non-homologous end joining (NHEJ) and the homologous recombination (HR). NHEJ operates on the broken phosphodiester linkages of the DNA throughout the cell cycle. HR repairs a DSB with an undamaged copy of the broken region.

These repair mechanisms only work up to a certain level of severity of the exposure to radiation. The damage to cells is divided into lethal, potentially lethal and a sublethal categories. Lethal damage leads to cell death, potentially lethal damages can be repaired under certain circumstances whereas sublethal damages are

repaired within hours. When multiple sublethal damages happen within a short period of time, it also leads to cell death [13].

1.9.1 Direct and Indirect Effects

Ionizing radiation causes:

- Loss of energy of radiation
- Production of ionization
- Excitation of atoms and molecules

As a result, free radicals are created within pico to femto seconds, which react with neighboring molecules and produce secondary DNA or lipid radicals. These are known to have a major role in the effects of radiation on biological tissues and organisms, as they contain highly reactive unpaired electrons [13].

Direct Effects

The free radicals may repair or cross-link due to a radical-radical reaction. Thus, they also react with oxygen. In the case of lipids, they initiate chain reactions for cell damage. An estimated one third of the biological damages are caused by direct effects [13].

Indirect Effects

The absorption of energy is connected to the abundance of material in the path of the radiation. Water, the most predominant molecule in a living organism, takes up a major proportion of the deposited radiation energy. Chemical changes, called water radiolysis, happen after exposure to radiation. This process can cause biological damage, as they are capable of diffusing in essential parts of the cell [13].

1.9.2 Fractionated Radiotherapy

The biological reason for fractionation is due to [13]:

- **Repair:**

  Healthy tissue has the possibility to overcome sublethal damages between each radiation session.

- **Repopulation:**

  Malignant and healthy cells proliferate caused by numerous cells damages, so they repopulate.

- **Redistribution:**

  Tumor cells redistribute in stages of the cell cycle where they are more radiosensitive, thus more can be killed.

- **Reoxygenation:**

  The more oxygen is in a tumor cell, the more biological damage can be caused by ionizing radiation.

In cancer therapy for sinonasal tumors in dogs, the two fractionation schemes typically used are:

Curative or definitive RT is designed to minimize long-term side effects of radiation and to improve the long-term control of cancer. Generally, this means giving small doses of radiation daily for two to four weeks. By performing many small radiation treatments, a large total radiation dose can be safely delivered.

Secondly, palliative RT, is designed to reduce cancer-related pain and to improve the patients' quality of life, but not to provide long-term tumor control. This type of treatment can be used in any dog with tumor-related clinical symptoms such as discomfort or bleeding. The daily dose delivered is higher, but the total dose is much lower than curative RT [45].

1.9.3 Cell Survival Curves

The definition of cell survival is the number of cells that keep their ability to reproduce e.g. after exposure to ionizing radiation.

The effect on cells after radiation exposure is measured by the surviving fraction (SF). To get SF measurements, a linear-quadratic (LQ) model is generally applied. SF is given as a function of absorbed dose D in Gy with the coefficients α as the proportionality factor to D in Gy^{-1} and β as the probability factor to D^2 in Gy^{-2}. Those parameters are determined as a function of accumulated dose.

$$SF = e^{-(\alpha D + \beta D^2)} \text{ with } D = \frac{\alpha}{\beta}$$

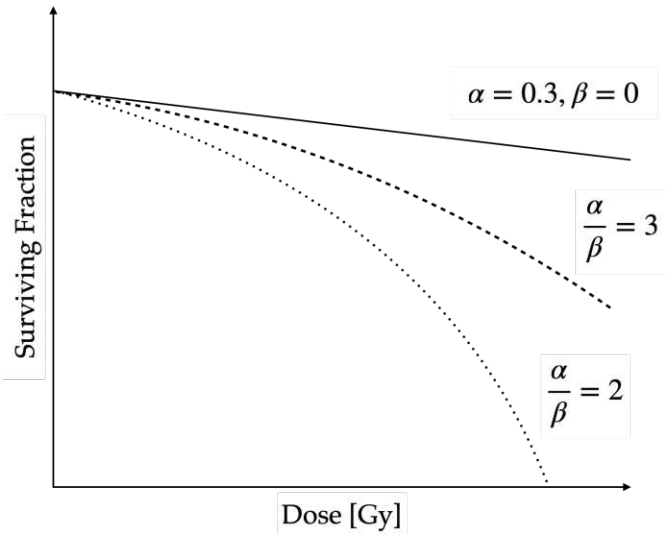

Fig. 16: Schematic cell survival curves for different α and β ratios. The lower the ratio, the higher SF is possible.

The ratio of α and β is the dose where the linear as well as the quadratic component cause the same amount of cell killing and determines whether tissue is radio-sensitive or radio-resistant. A higher ratio leads to a more linear cell survival curve. Conversely, a lower ratio (high beta relative to alpha), leads to a more curved cell survival curve. This is important, as tissues with a low ratio are relatively resistant to low doses in contrast to tissues with a high ratio. Most tumors, except e.g. melanomas, sarcomas and prostate cancer have a high ratio and can

therefore be exposed to higher single doses to achieve a better tumor control with approximately the same side effects [13], [46], [47].

1.10 Aim of Thesis

The aim of this master's thesis is to apply the improvements of modern radiation techniques in veterinary radiooncology.

The University of Veterinary Medicine Vienna is currently using 3D-RT, but is investing in a new Linac system capable of delivering VMAT treatment plans. The Department of Radiation Oncology of the Medical University Vienna / General Hospital of Vienna (AKH) has a wide range of experience with complex and modern radiation techniques for the human body. Hence, the University of Veterinary Medicine Vienna has a high interest of transferring the knowledge gained in the human oncology department for treating tumors in the veterinary field.

By nature, the anatomy of animals is very different from the human body. Target areas are smaller; organs of risk as well as the location of organs are not identical. Consequently, tumor treatments in veterinary medicine are a challenging task. Because of this, the goal for this thesis is to investigate the advantages from VMAT for dogs with tumors in the head area, especially sinonasal tumors in an in-silico treatment planning study.

The main task is to compare the doses the PTVs and the OARs received during 3D-RT and VMAT. The 3D-RT plans as well as the CT images of the patients were provided by the University of Veterinary Medicine Vienna, whereas the VMAT treatment plans were development with RayStation 11A in the MUW/AKH. Further tasks include the calculation of dosimetric limits for the dogs OARs and the measurements of the plans on a phantom with the Linac of the MUW/AKH.

2 Materials and Methods

2.1 Linear Accelerators

Siemens Primus Mid Energy

Fig. 17: Siemens Primus Mid Energy

RT treatments at the University of Veterinary Medicine Vienna were performed until May 2022 by a Siemens Primus Mid Energy linac producing 6 *MV* photon beams, as seen in Figure 17.

The 3D-RT plans with this machine commonly used parallel opposed beams collimated by shielding blocks. The beam has a constant intensity. Consequently, PTV-surrounded healthy organs and tissues are not as easily spared.

ELEKTA Infinity

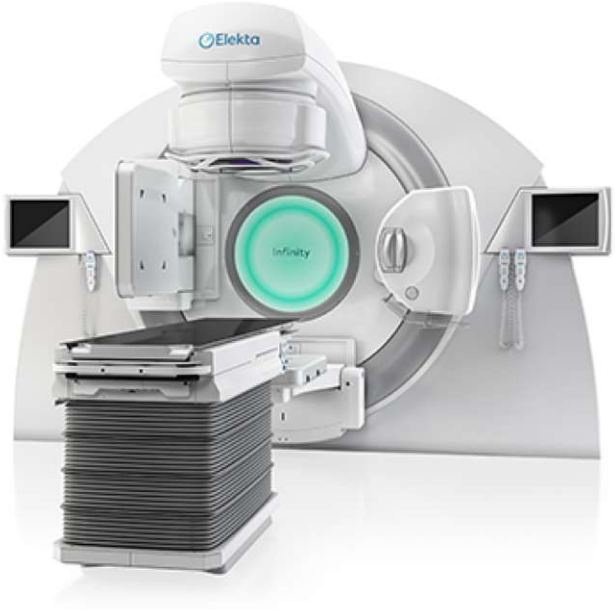

Fig. 18: Sample Picture of an ELEKTA Infinity Linac. Source: [48]

The new Linac procured by the University of Veterinary Medicine Vienna is shown in Figure 18. Infinity (ELEKTA AB, Stockholm, Sweden) Linac is equipped with an Agility™ MLC, that consists of $80 \times 5\ mm$ tungsten leaf pairs across a $40 \times 40\ cm^2$ field. The leaves can speed up to 6.5 cm/s. Also, the MLC is designed with an ultra-low radiation leakage system. Due to the fast leaf speeds, the patient can be treated more rapidly.

The photon beams can be flattened with a filter, or operated in a high dose rate mode without a flattening filter.

The gantry head can move around up to 360° and is equipped with a motorized wedge. The gantry speed is also adjustable, as well as the dose rate. [49]

2.2 Primary Data

The University of Veterinary Medicine Vienna provided the CT-based 3D-RT plans of all canine patients. Those plans and CT images gave information about the PTVs, GTVs, CTVs and OARs, their volumes as well as the 3D-RT beam set-ups. For each patient, a palliative and definitive treatment plan was provided. The palliative treatment plans were used for pain relief related to the tumor, but not full curation of the disease. Definitive plans, on the other hand, were the plans to get full control of the tumor with the intent to fully cure the patient. In definitive plans, the PTVs got a $15 \times 3.2\ Gy = 48\ Gy$ dose. In palliative plans, the PTVs got a $5 \times 4\ Gy = 20\ Gy$ dose.

2.3 Patient Cohort

Eleven dogs with sinonasal tumors were included in this study. Their clinical data is shown in Table 2:

	Age	**Sex**	**Weight [kg]**	**Breed**	**Tumor Type**	**Adam's Stage**
Patient 1	12	Female, castrated	29,8	Labrador	Adenocarcinoma	2
Patient 2	12	Female, castrated	6,6	Mix	Adenocarcinoma	3
Patient 3	9	Male, castrated	34,3	Mix	Adenocarcinoma	4
Patient 4	11	Female, castrated	22,9	Münsterländer	Adenoid carcinoma	4

Patient 5	9	Male	10,9	Border Terrier	Adenocarcinoma	4
Patient 6	9	Female, castrated	24,9	Mix	Transitional epithelial carcinoma	3
Patient 7	3	Male, castrated	45	Berner Sennen	Chondrosarcoma	2
Patient 8	9	Male, castrated	31,3	Labrador	Fibrosarcoma	2
Patient 9	6	Female, castrated	21,8	Staffordshire Terrier	Chondrosarcoma	4
Patient 10	9	Female, castrated	24,7	Hungarian Bracke	Transitional epithelial carcinoma	3
Patient 11	4	Male	25,2	Husky	Chondrosarcoma	4

T. 2: Patient Cohort.

The eleven patients belonged to different dog breeds with an average weight of 25,2 kg. The average age was 9 years. Six female and 5 male dogs were treated with RT. Clinical disease (modified Adams system) varied from stage 2 to 4. The most common tumor type was a nasal adenocarcinoma.

2.4 Treatment Planning with RayStation 11A

The accurate dose calculation and the general outcome of the RT is strongly influenced by the planning system. The systems beam model accuracy and the critical validation are crucial for an advanced treatment technique.

RayStation 11A, developed by RaySearch Medical Laboratories AB in Stockholm, Sweden offers a software system for the complex demands that are necessary for this thesis.

2.4.1 PTV, CTV, GTV

The important treatment volumes explained in chapter 1.6.3 need correct contouring, as it is essential in RT planning. The GTV, CTV and PTV are number 1, 2 and 3 in Figure 20.

First the gross tumor volume (GTV) was contoured, because it is the actual visible tumor. After that, the clinical target volume (CTV) was created by an automatic expansion, also called margin. Lastly, the planning target volume (PTV) was added to the CTV with a margin.

The PTV is the target volume and the region of interest in the planning system, that gets the full radiation dose during RT.

2.4.2 OARs

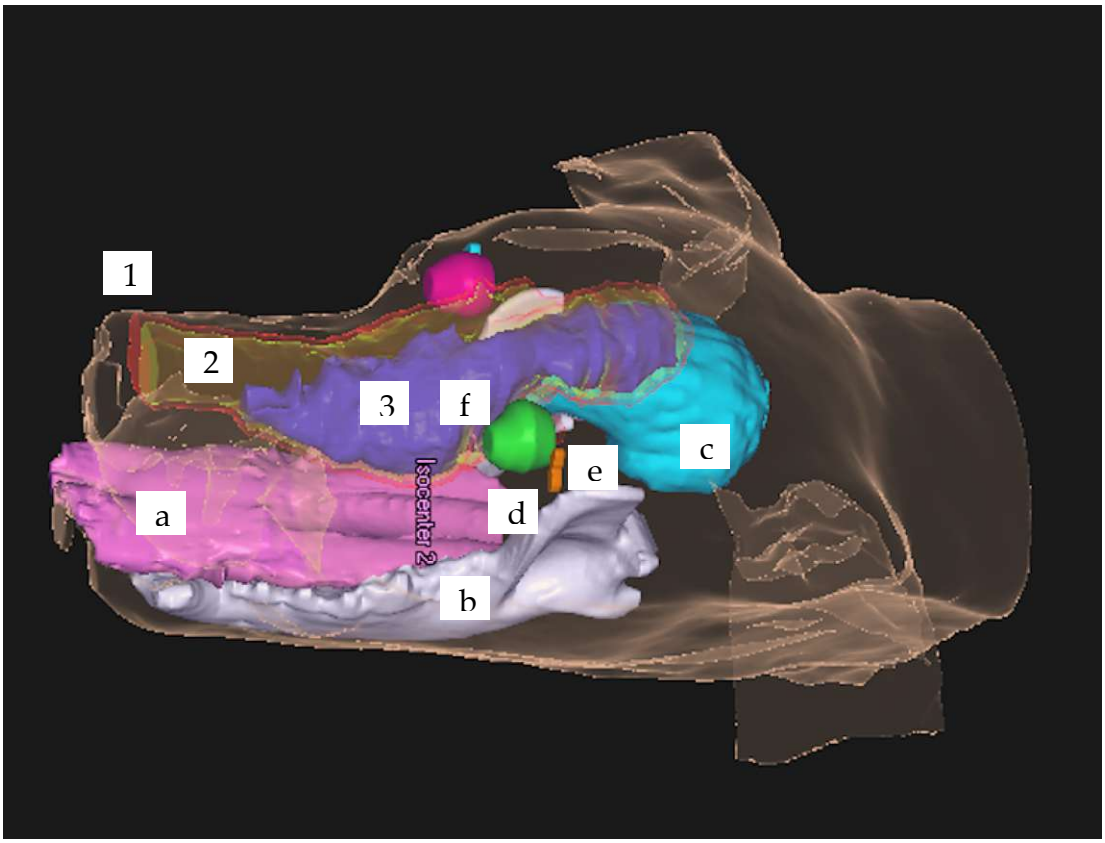

Fig. 19: Sample picture of a patient with contoured OARs and PTV, CTV, and GTV.

1. PTV
2. CTV
3. PTV

a. Tongue
b. Lower Jaw Bone
c. Brain
d. Eye (Ipsilateral + Contralateral)
e. Lacrimal Gland (Ipsilateral + Contralateral)
f. Eye Lens (Ipsilateral + Contralateral)

Described in Section 1.6.3, OARs are healthy tissues and organs that must to be spared during RT. In total, 9 OARs were contoured for each of the 11 patients.

Ipsilateral means that the organ is located on the same side as the tumor, contralateral means is on the other side.

Based on the dosimetric limits constraints of human OARs, the constraints for the OARs of dogs were calculated with the Withers formula [50]:

$$EQD_2 = D\left[\frac{d + {}^{\alpha}/_{\beta}}{2 + {}^{\alpha}/_{\beta}}\right]$$

where EQD_2 is the dose delivered in 2 Gy fractions that is biologically equivalent to the total dose. D is the total dose given in Gy, d is the dose per fraction in Gy.

The alpha/beta-ratio used, described in Section 1.9.3, was 3 for organs and 2 for organs and tissues where nerves are involved.

The calculated values of each OAR were used as an orientation during treatment planning.

2.4.3 Beam Setup

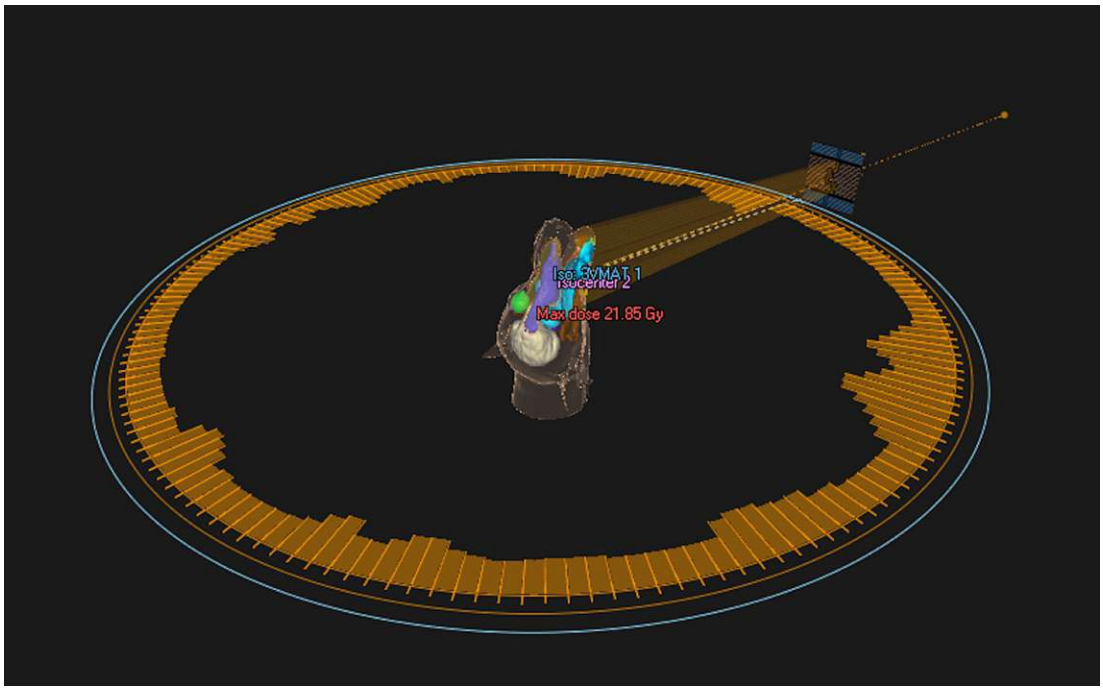

Fig. 20: Sample picture of the used beam setup.

The beam setup had the primary goal to achieve a uniform dose distribution to the target and fulfillment of the clinical goals at the same time.

All VMAT plans for the 11 patients, palliative ($5 \times 4\ Gy = 20\ Gy$) and definitive ($15 \times 3.2\ Gy = 48\ Gy$), had the same setup. Two beams irradiated the patient:

In beam 1, the collimator seen in Figure 21, a 358° clockwise arc was used. The gantry started at 181 [deg] and ended at 179 [deg]. The rotation of the collimator and the couch was 0°.

In beam 2, the collimator seen in Figure 22, a 358° counterclockwise arc was used. The gantry started at 179 [deg] and ended at 181 [deg] with a collimator rotation of 30° and a couch rotation of 0°.

Additionally, all beams had a maximum dose rate limit of 500 monitor units. A gantry spacing of 2° was used for both arcs.

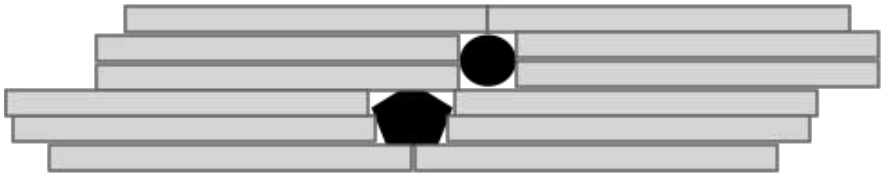

Fig. 21: Schematic picture of a 0° collimator angle.

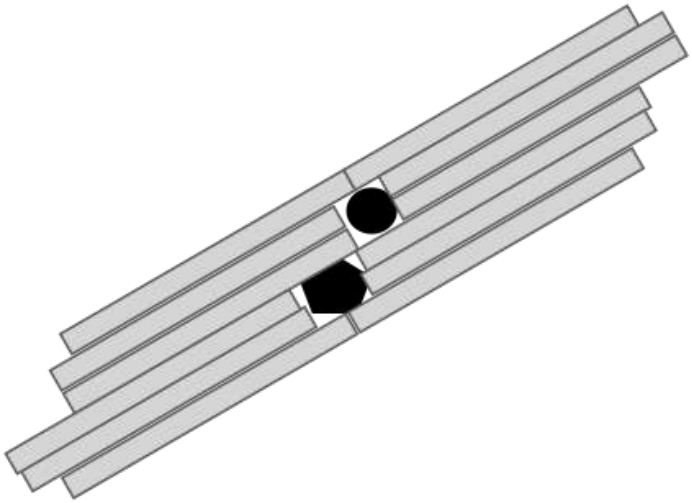

Fig. 22: Schematic picture of a 30° collimator angle.

2.4.4 Plan Design

To optimize the VMAT plans, RayStation provides optimization functions. Each function can be weighted, to rank their importance in the RT planning process. Also, functions can be handed as objectives or constraints. The following functions were used in the plans and are from the User Manual of RayStation 11A:

Min/Max Dose:

The Min Dose function increases the dose in the entire region of interest (ROI), so that each volume receives at least the specified dose. The Min Dose function can only be used for a target structure (GTV, CTV or PTV), because only these structures can increase the dose to a certain level.

Conversely, the Max Dose function reduces the maximum dose in the volume to the specified dose level. Max Dose is available for target structures and OARs.

The Min/Max functions can be used in the same volume at the same time, to avoid under- or overradiation.

Min/Max DVH:

DVH functions either raise or lower the dose in a percentage of a volume, but it is not possible to influence a specific region as no special information is available.

Dose-Fall-Off:

The dose-fall-off function starts at a high dose level defined at the edge of the ROI and linearly reduces the dose within a certain distance to a certain low dose level. It behaves like a maximum dose function but decreases with high dose and increases with low dose distance. Hence, OARs next to the PTV get their dosimetric limits with this function.

2.5 Statistical Analysis

A Student's t-test is a tool to compare the means of one or two populations. The observation in one sample can be paired with observations in the other sample.

For this thesis, the dose difference between the dosimetric parameters of PTVs and OARs of the 3D-RT and the VMAT plans were statistically evaluated. Hence, a paired t-test was performed. As each patient had the same PTVs and OARs in the 3D-RT- and VMAT-plans, the measurements were dependent.

Like many statistical procedures, the paired t-test has two hypotheses: the null and the alternative hypothesis. The null hypothesis H_0 assumes that the true mean difference is equal to zero, whereas the alternative H_1 assumes that it is not equal to zero. [51]

The paired t-test was carried out in following steps [51]:

1. Calculation of the difference between the two observations on each pair:
$$d_i = y_i - x_i$$
2. Calculation of the mean difference, $\bar{d}$
3. Calculation of the standard deviation of the differences, s_d to calculate the standard error of the mean difference:
$$SE(\bar{d}) = \frac{s_d}{\sqrt{n}}$$
4. Under the null hypothesis, the statistic followed a t-distribution with $n - 1$ degrees of freedom with following formula:
$$T = \frac{\bar{d}}{SE(\bar{d})}$$
5. The value of T was compared to the t_{n-1} distribution table to give the P value.
6. The alpha value, also called significance level, was predefined at 0.05. It indicates a 5% risk of concluding that a difference exists when there is no actual difference.

7. When the calculated P value was smaller than alpha, H_1 was chosen. Vice versa, H_0 was not rejected.

2.6 Target Coverage

RayStation 11A gave the target coverage in Gy-values to evaluate the plans with following parameters:

- $D99 = D_{min}$: 99% of the ROI volume cm^3 received at least a dose of ... Gy
- $D98$: 98% of the ROI volume cm^3 received at least a dose of ... Gy
- $D95$: 95% of the ROI volume cm^3 received at least a dose of ... Gy
- $D_{Average}$: Mean dose of the ROI volume cm^3 received at least a dose of ... Gy
- $D50$: 50% of the ROI volume cm^3 received at least a dose of ... Gy
- $D2$: 2% of the ROI volume cm^3 received at least a dose of ... Gy
- $D1 = D_{max}$: 1% of the ROI volume cm^3 received at least a dose of ... Gy

For evaluation of the improvements from 3D-RT to VMAT, different target coverage parameters were used for the OARs. Table 3 shows the used target coverage for each OAR. The maximal dose $D1 = D_{max}$ was used for more radiation-sensitive organs, the average dose $D_{Average}$ for less radiation-sensitive organs.

Brain	D_{max}
Ipsilateral Eye	$D_{Average}$
Ipsilateral Lacrimal Gland	$D_{Average}$
Ipsilateral Lens	D_{max}
Contralateral Eye	$D_{Average}$
Contralateral Lacrimal Gland	$D_{Average}$
Contralateral Lens	D_{max}
Lower Jaw	D_{max}
Tongue	$D_{Average}$

T. 3: Target coverages for each OAR.

2.7 Patient specific plan verification

The calculated dose distributions with RayStation 11A were measured on an ELEKTA Versa HD Linac of the MUW/AKH with the Delta4 Phantom+ using the γ-index technique for evaluation of the plans. The used parameter, the gamma pass rate (GPR), was calculated for each point of interest using the preselected dose difference (DD) and distance to agreement (DTA). A GPR under 90% for 2% DD and 2*mm* DTA was a pass/fail criterion for each plan [52].

3 Results

3.1 Calculated Constraints

In chapter 2.4.2, the formula for OAR dose constraints calculations was introduced. The used alpha/beta-ratio, described in 1.9.3, was 3 for organs and 2 for organs and tissues with nerve-involvement and calculated for both.

The resulting values are shown in Table 4.

OAR		**Human [Gy]**	**Dog [Gy]** $\alpha/\beta = 2$	**Dog [Gy]** $\alpha/\beta = 3$
Brain	D_{max}	60	47	44
Lacrimal Gland	$D_{Average}$	26	20	19
Lens	D_{max}	25	19	18
	D_{max}	5	4	4
Eye	D_{mean}	35	27	25
	D_{max}	50	38	36
Lower Jaw	D_{max}	55	42	39
Tongue	D_{mean}	40	31	29

T. 4: Table of calculated constraints.

The calculated constraints were exceeded multiple times. How often the dose value from the patient cohort was higher than the dosimetric limit per treatment technique and OAR is shown in Table 5.

OAR	Definitive 3D-RT	Palliative 3D-RT	Definitive VMAT	Palliative VMAT
Brain	10	0	4	0
Ipsilateral Eye	11	0	0	0
Ipsilateral Lacrimal Gland	4	1	1	0
Ipsilateral Lens	11	8	2	0
Contralateral Eye	4	0	0	0
Contralateral Lacrimal Gland	2	0	0	0
Contralateral Lens	9	3	0	0
Lower Jaw	11	0	0	0
Tongue	9	0	0	0

T. 5: Number of dosimetric limit excesses of the patient cohort.

3.2 Planning Target Volume (PTV)

PTV	Definitive Plans		Palliative Plans	
	3D-RT [Gy]	VMAT [Gy]	3D-RT [Gy]	VMAT [Gy]
Mean of $D_{Average}$	48,4	48,7	20,1	20,1
Standard Deviation	0,5	0,2	0,3	0,1
Max	49,4	49,2	20,6	20,4
Min	47,8	48,3	19,4	20,0
IQR: Q1	48,1	48,6	20,0	20,1
IQR: Q3	48,7	48,8	20,3	20,1
P-Value	0,113		0,992	
Alpha	0,05		0,05	
Hypothesis	H_0 not rejected		H_0 not rejected	

T. 6: 3D-RT and VMAT PTV $D_{Average}$-values, definitive and palliative.

For the 3D-RT and VMAT definitive plans, the clinical PTV goal was to deliver an $D_{Average}$ dose of 48 Gy in 15 sessions with a 3.2 Gy dose per fraction. In direct comparison, the VMAT-plans had a marginally higher mean, a smaller standard deviation, a lower maximum and a higher minimum than the 3D-RT-plans. The interquartile range (IQR) for the VMAT-plans was also smaller than the 3D-RT-plans. The resulting p-value of the student's t-test was higher than the significance level. Therefore, H_0 was not rejected and no significant difference was found.

For the 3D-RT and VMAT palliative plans, the clinical goal for the PTV was to deliver an $D_{Average}$ dose of 20 Gy in 5 sessions with a 4 Gy dose per fraction. 3D-

RT-plans and VMAT-plans had the same mean. The standard deviation, the maximum and the IQR were smaller for VMAT-plans. The minimum dose was higher for VMAT-plans compared to 3D-RT-plans. The resulting p-value of the students t-test was higher than the significance level alpha. Therefore, H_0 was not rejected and no significant difference was found.

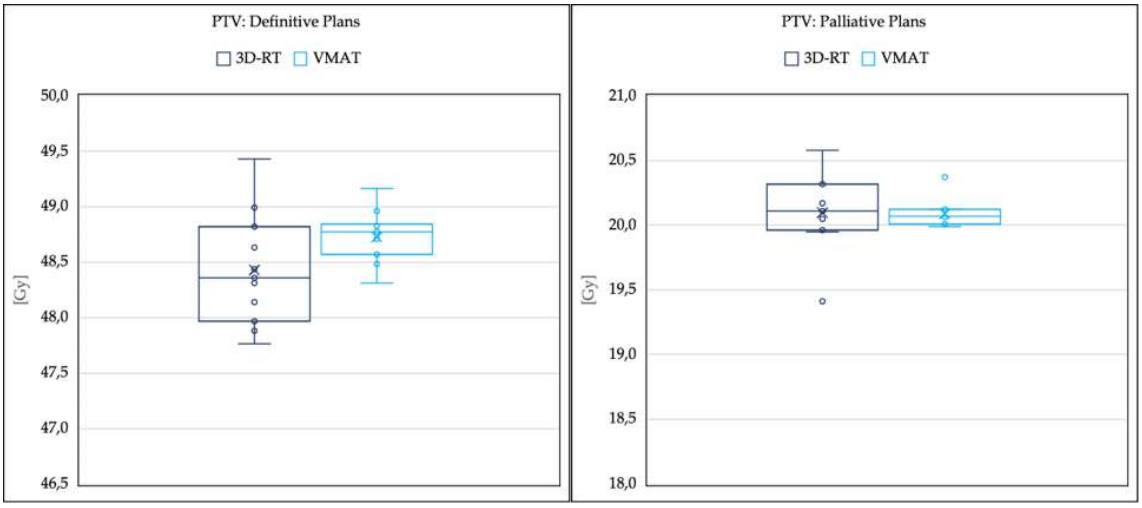

Fig. 23: Box-plot of 3D-RT and VMAT PTV-values for definitive and palliative plans.

3.3 Organs at Risk (OARs)

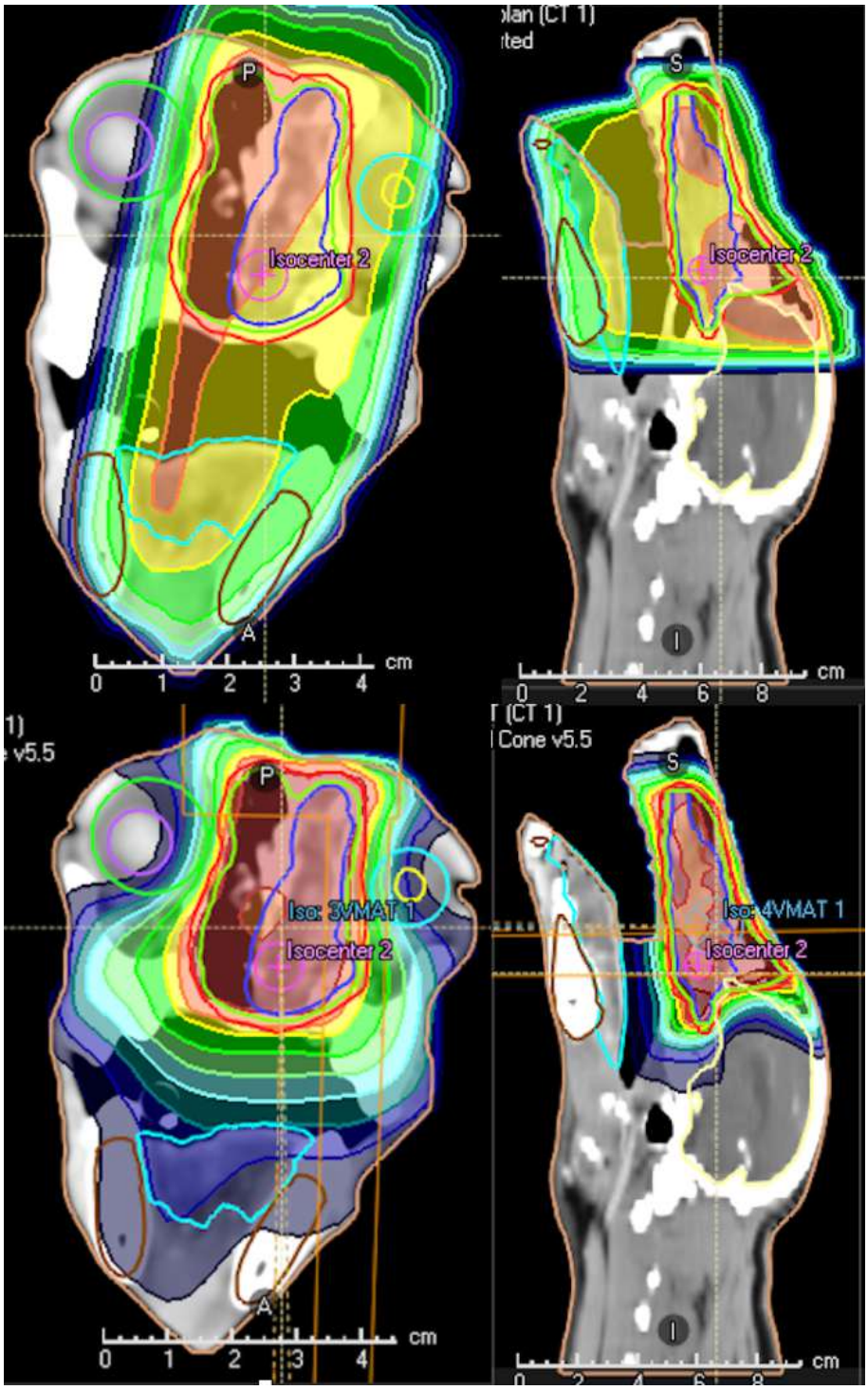

Fig. 24: Comparison of a 3D-RT treatment plan (upper left and right image) and a VMAT treatment plan (lower left and right image), shown on a patient in the frontal plane (left) and sagittal plane (right).

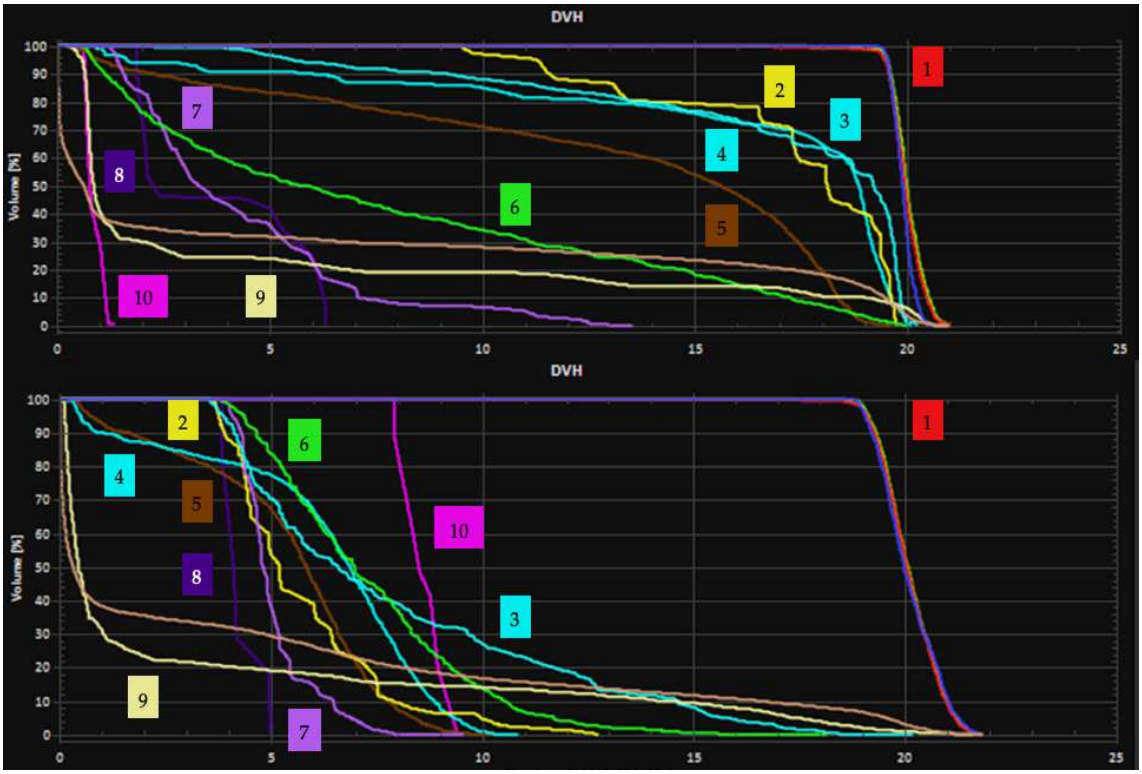

Fig. 25: Example of a palliative DVH of 3D-RT treatment plan (upper image) compared to a VMAT treatment plan (lower image).

1. PTV, GTV, CTV
2. Ipsilateral Lens
3. Ipsilateral Eye
4. Tongue
5. Lower Jaw
6. Contralateral Eye
7. Contralateral Lens
8. Contralateral Lacrimal Gland
9. Brain
10. Ipsilateral Lacrimal Gland

Figure 25 illustrates the DVHs of the same patient shown in Figure 24, both palliative ($5 \times 4\ Gy = 20\ Gy$) irradiated. The upper graph shows the 3D-RT DVH, the lower one the VMAT DVH. This figure serves only an example to illustrate the differences between the two irradiation techniques in a DVH. First and foremost, the PTV was did not change significantly. At the same time, a larger difference was visible in the OARs, such as the lower jaw (brown) or the ipsilateral lens (yellow).

A summary of the calculated doses for each OAR is shown in Table 7:

	Definitive Plans $15 \times 3.2\ Gy = 48\ Gy$			**Palliative Plans** $5 \times 4\ Gy = 20\ Gy$		
	3D-RT [Gy]	**VMAT [Gy]**	**P-Value**	**3D-RT [Gy]**	**VMAT [Gy]**	**P-Value**
Brain	45,8 ± 12,5	41,3 ± 12,4	<0,05	19,2 ± 5,3	17,9 ± 5,3	<0,05
Ipsilateral Eye	40,8 ± 7,7	14,2 ± 4,7	<0,05	17,0 ± 3,2	9,5 ± 1,2	<0,05
Ipsilateral Lacrimal Gland	19,5 ± 18,3	9,7 ± 4,1	N.S.	8,2 ± 7,7	5,3 ± 1,1	N.S.
Ipsilateral Lens	46,0 ± 4,4	15,8 ± 6,1	<0,05	18,8 ± 2,1	11,7 ± 2,5	<0,05
Contralateral Eye	20,1 ± 8,0	11,1 ± 1,6	<0,05	8,4 ± 3,4	9,0 ± 1,7	N.S.
Contralateral Lacrimal Gland	7,6 ± 8,4	8,5 ± 2,2	N.S.	3,2 ± 3,6	6,0 ± 1,6	<0,05
Contralateral Lens	31,5 ± 12,5	12,9 ± 2,8	<0,05	12,1 ± 6,0	11,7 ± 2,9	N.S.
Lower Jaw	48,6 ± 1,9	13,8 ± 1,4	<0,05	18,8 ± 4,5	8,2 ± 0,8	<0,05
Tongue	36,3 ± 7,6	8,9 ± 1,0	<0,05	15,1 ± 3,3	5,6 ± 0,7	<0,05

T. 7: Summary of all OARs; N.S.: not significant.

The highest significant difference was found for the tongue and lower jaw for both definitive and palliative plans. Conversely, the lowest significant difference was found for the contralateral lacrimal gland for both definitive and palliative plans. Also, the brain had a low significant difference for the definitive plans and the contralateral eye for the palliative plans.

3.3.1 Brain

	a) Definitive Plans $\mathbf{15 \times 3.2\ Gy = 48\ Gy}$		**b) Palliative Plans** $\mathbf{5 \times 4\ Gy = 20\ Gy}$	
	3D-RT [Gy]	**VMAT [Gy]**	**3D-RT [Gy]**	**VMAT [Gy]**
Mean of D_{max}	45,8	41,2	19,2	17,9
Standard Deviation	13,1	12,9	5,6	5,6
Max	50,9	49,0	22,0	20,1
Min	6,2	2,9	2,5	1,3
IQR: Q1	49,1	42,8	20,4	19,2
IQR: Q3	50,2	47,2	21,2	20,0
P-Value	6,17679E-05		0,00353881	
Alpha	0,05		0,05	
Hypothesis	H_0 rejected		H_0 rejected	

T. 8: Dose-values of the brain in definitive and palliative 3D-RT- and VMAT-plans.

The calculated dosimetric limit for the brain was at 47 Gy. Hence, with both treatment types, the mean D_{max} value did not exceed the dosimetric limit.

For both plan types, VMAT shares a lower mean, maximum, minimum and IQR than the 3D-RT-plans. The standard deviation for definitive VMAT plans was also lower, whereas for the palliative plans the standard deviation was on the same level.

Both p-values were much smaller than the significance level alpha of 0,05, therefore the hypothesis H_1 was accepted and a significant difference could be statistically proven for both plans.

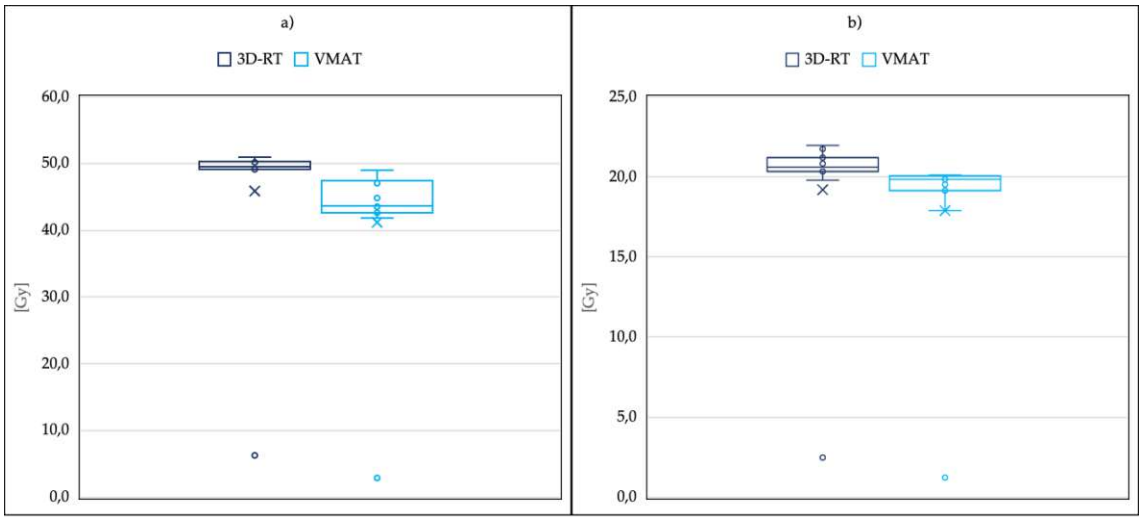

Fig. 26: Box-plots of 3D-RT and VMAT [Gy]-values of the brain: a) Definitive plans, b) Palliative plans.

3.3.2 Contralateral Lacrimal Gland

	a) Definitive Plans $15 \times 3.2\ Gy = 48\ Gy$		b) Palliative Plans $5 \times 4\ Gy = 20\ Gy$	
	3D-RT [Gy]	**VMAT [Gy]**	**3D-RT [Gy]**	**VMAT [Gy]**
Mean of $D_{Average}$	7,6	8,4	3,2	6,0
Standard Deviation	8,8	2,2	3,7	1,7
Max	24,8	11,1	10,9	8,0
Min	1,7	4,0	0,7	3,0
IQR: Q1	2,1	7,3	0,9	5,2
IQR: Q3	11,1	9,7	4,5	7,0
P-Value	0,772051456		0,02851207	
Alpha	0,05		0,05	
Hypothesis	H_o not rejected		H_0 rejected	

T. 9: Dose-values of the contralateral lacrimal gland in definitive and palliative 3D-RT- and VMAT-plans.

Located next to the contralateral eye, the calculated dosimetric limit for the contralateral lacrimal gland of 19 Gy was not exceeded by the mean $D_{Average}$ of 3D-RT or VMAT plans. Although the maximum value for the definitive 3D-RT plan was higher than the maximum value for the definitive VMAT plan, the lower mean and minimum values led to the non-rejection of H_0.

Although the minimum and mean value for the palliative 3D-RT-plans were lower, H_0 rejected due to the higher maximum value in comparison to the VMAT-plans.

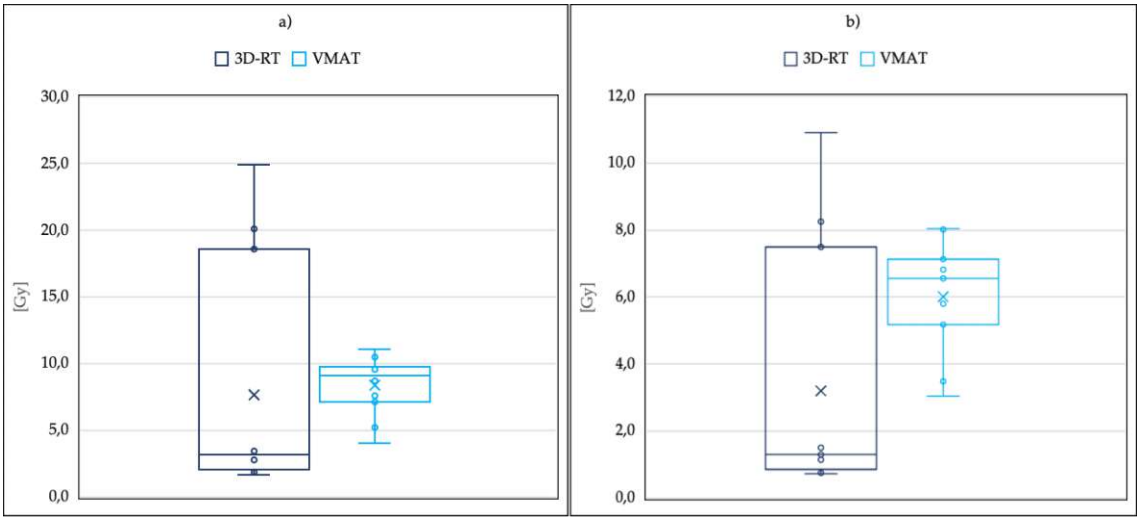

Fig. 27: Box-plots of 3D-RT and VMAT Gy-values of the contralateral lacrimal gland: a) Definitive plans, b) Palliative plans.

3.3.3 Lower Jaw

	a) Definitive Plans $15 \times 3.2\ Gy = 48\ Gy$		b) Palliative Plans $5 \times 4\ Gy = 20\ Gy$	
	3D-RT [Gy]	**VMAT [Gy]**	**3D-RT [Gy]**	**VMAT [Gy]**
Mean of D_{max}	48,6	13,8	18,8	8,2
Standard Deviation	1,9	1,4	4,8	0,8
Max	51,5	16,0	21,0	9,2
Min	45,5	11,0	4,5	6,6
IQR: Q1	47,6	13,4	19,5	7,8
IQR: Q3	50,0	14,2	20,4	8,8
P-Value	1,09743E-12		1,5811E-05	
Alpha	0,05		0,05	
Hypothesis	H_0 rejected		H_0 rejected	

T. 10: Dose-values of the lower jaw in definitive and palliative 3D-RT- and VMAT-plans.

The lower jawbone is located under the PTV in the patients' head. The calculated dosimetric limit was at 39 Gy, which was only exceeded by the definitive mean D_{max} of the 3D-RT plans.

For the definitive and palliative plans, all values for the VMAT-plans were lower. H_0 was rejected for both and a significant difference could be found.

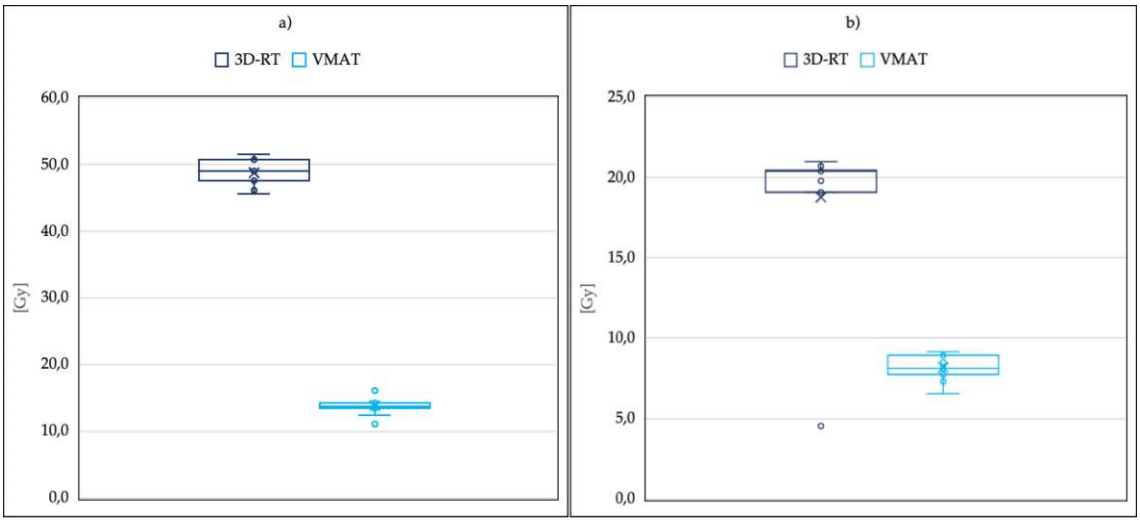

Fig. 28: Box-plots of 3D-RT and VMAT Gy-values of the lower jaw: a) Definitive plans, b) Palliative plans

3.3.4 Tongue

	a) Definitive Plans $15 \times 3.2\ Gy = 48\ Gy$		b) Palliative Plans $5 \times 4\ Gy = 20\ Gy$	
	3D-RT [Gy]	**VMAT [Gy]**	**3D-RT [Gy]**	**VMAT [Gy]**
Mean of $D_{Average}$	36,3	8,9	15,1	5,6
Standard Deviation	8,0	1,1	3,5	0,7
Max	45,9	11,2	19,3	6,6
Min	16,4	7,1	6,8	4,7
IQR: Q1	37,3	8,4	15,4	5,0
IQR: Q3	39,6	9,1	16,7	6,2
P-Value	4,37455E-07		3,1476E-06	
Alpha	0,05		0,05	
Hypothesis	H_0 rejected		H_0 rejected	

T. 11: Dose-values of the tongue in definitive and palliative 3D-RT- and VMAT-plans.

The tongue is located under the PTV and next to the lower jawbone. The calculated dosimetric limit was 29 Gy. Except the mean $D_{Average}$ of the definitive 3D-RT plans, all others were within the limit.

Both definitive and palliative VMAT-plans had all values lower than the 3D-RT plans.

Therefore, H_0 was rejected for both definitive and palliative treatment plans and a significant difference could be found.

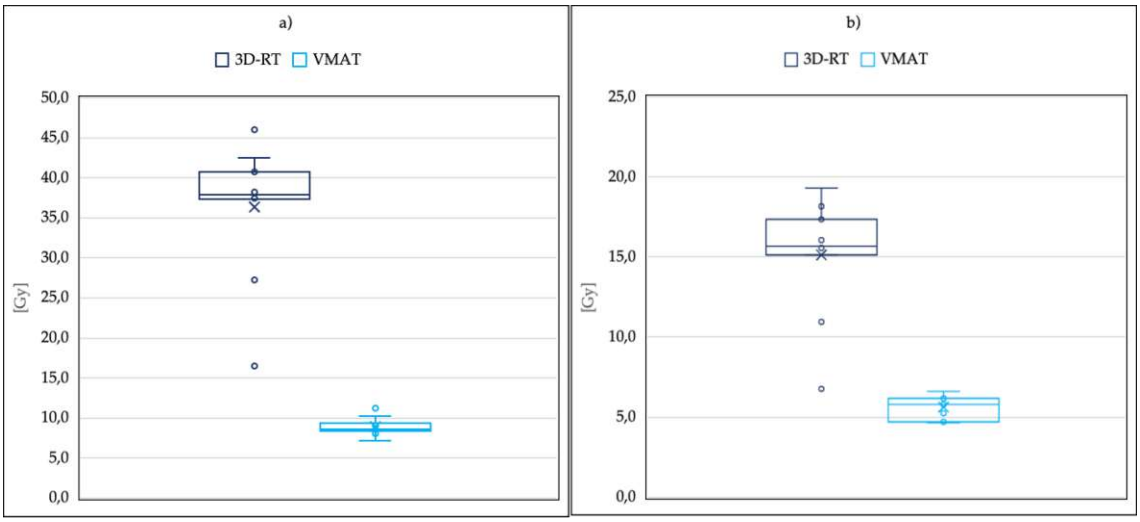

Fig. 29: Box-plots of 3D-RT and VMAT Gy-values of the tongue: a) Definitive plans, b) Palliative plans.

3.4 Patient specific plan verification

All VMAT plans reached an average of the GPR for 2%, 2mm of 92,8% ± 2,8%. Furthermore, the GPR for 3%, 3 mm was at 98,4% ± 1,5%. Consequently, each plan passed the pass criterion. Therefore, the VMAT plans created in RayStation 11A can be implemented in practice.

4 Discussion

For the patient cohort discussed in Section 2.3, VMAT delivery based treatment plans were employed and developed in RayStation 11A.

In general, the given 3D-RT and the achieved VMAT dose distributions have shown variations, which was partly caused by the patient cohort. The treated patients were 4 males and 7 females, had an average weight of 25,2 kg ± 11,1 kg, an average age of 9,4 years ± 3,0 years and therefore differed in weight, size, shape, dog race. Tumor stages were also divergent, as three patients had Adam's Stage 2 tumors, three Stage 3 and four had Stage 4.

The obtained data suggests that there was an improvement between VMAT and 3D-RT:

- VMAT had the same level of accuracy for PTV coverage, but was irradiating the surrounding healthy organs and tissues not as intensely as 3D-RT.
- The dosimetric limit for the OARs were exceeded more often for 3D-RT plans compared to VMAT plans.
- For the definitive plans, 7 out of 9 OARs rejected H_0 when statistically tested with the students t-test. For the palliative plans, 6 out of 9 OARs respectively.

4.1 Planning Target Volume

The PTV goals of $D_{Average} \sim 48\ Gy$ for the definitive and $D_{Average} \sim 20\ Gy$ for the palliative treatment could be fulfilled by both VMAT and 3D-RT treatment plans, which is depicted in Table 6.

In direct comparison, a smaller dose variation was observed for VMAT treatment plans, as VMAT had a smaller IQR. This was not surprising for VMAT delivery.

VMAT generates a highly conformal treatment field with the dose delivered continuously as the Linac rotates around the patient. Therefore, it was possible to irradiate very irregular PTV shapes in a highly conformal manner.

Nevertheless, 3D-RT also achieved these goals, but at the expense of an increased dose exposure to the OARs.

4.2 Organs at Risk

As depicted in Figure 24 in Section 3.3, it was more challenging in 3D-RT compared to VMAT, to find the right balance between an adequate dose distribution for which the PTV coverage was high and the dose exposure to the OARs was as low as achievable. The 3D-RT Linac did not use a MLC and only had parallel opposed shielding blocks. Dependent on the location of the PTV within the treatment field, a higher PTV coverage was chosen over a low dose exposure, if it was not possible to achieve both conditions equally. Generally, in clinical situations when it is not possible to achieve neither a high PTV coverage nor a low dose exposure of OARs, because of reasons like anatomical properties of the patient, or the shape and the location of the PTV, VMAT might therefore be the better choice for dose delivery.

4.2.1 Tongue and Lower Jaw

Compared to the other OARs, the largest difference between the 3D-RT and VMAT plans were observed in the tongue and the lower jaw in all 11 patients. The delivered average dose from the 3D-RT to the VMAT plans in the tongue for the definitive plans was lowered by 76% and 72%, respectively, in the lower jaw. The palliative plans showed similar results, as the delivered average dose was reduced by 63% for the tongue and by 56% for the lower jaw.

Figure 24 in Section 3.3 depicts an example of the outcome of a 3D-RT treatment plan compared to the outcome of a VMAT treatment plan. While the 3D-RT dose distribution was nearly constant throughout the tongue and lower jaw located under the PTV, the VMAT technique spared those areas almost in its entirety.

Therefore, the benefits of the VMAT technique in comparison to 3D-RT, such as the adjustable dose rate, rotation speed and gantry and the size and shape adaptation during treatment are most obvious in the tongue and lower jaw.

4.2.2 Contralateral Lacrimal Gland

Out of all OARs, the smallest difference between the 3D-RT and VMAT plans was observed in the contralateral lacrimal gland. For the definitive plans, the average mean dose increased from 7,6 Gy in the 3D-RT plans to 8,5 Gy in the VMAT plans, resulting in a 11% increase between the treatment techniques. The palliative plans had an average mean dose of 3,2 Gy for the 3D-RT and 6,0 Gy for the VMAT plans, resulting in an increase of 89%.

As Figure 24 in Section 3.3 illustrates, the 3D-RT treatment was using shielding blocks to spare the OARs, leading to a sharp edge of the dose distribution on the contralateral side of the patient. Therefore, the contralateral lacrimal gland was spared effectively. As the VMAT treatment technique was irradiating the patient with a 360° gantry, the low dose exposure of the body was increased.

However, VMAT leads to highly conformal dose distributions in general and therefore in none of the definitive and palliative plans the dosimetric limit was exceeded for the contralateral lacrimal gland, compared to the 3D-RT plans, which exceeded the limit multiple times.

4.2.3 Brain

A small difference between the 3D-RT and VMAT dose distribution in the brain was also observed. For the definitive plans, the average mean D_{max} dose distribution was at 45,8 Gy for the 3D-RT plans and at 41,3 Gy for the VMAT plans, leading to a 10% decrease between the treatment types.

Depending on their stage, tumors of the nasal cavity and sinonasal tumors can invade through the cribriform plate into the brain, potentially causing neurologic signs [40].

Figure 24 in Section 3.3 shows that the shielding blocks in the 3D-RT spared out the brain effectively, but are not able to adapt to the shape of the brain as precisely as VMAT did. Also, due to possible overlap of the brain with the PTV depending on the tumor stage, only a small difference was found.

4.2.4 Dose Constraints

The clinical goals given in Table 4 for the 11 patients were exceeded for most of the OARs in 3D-RT compared to the VMAT plans, shown in Figure 30.

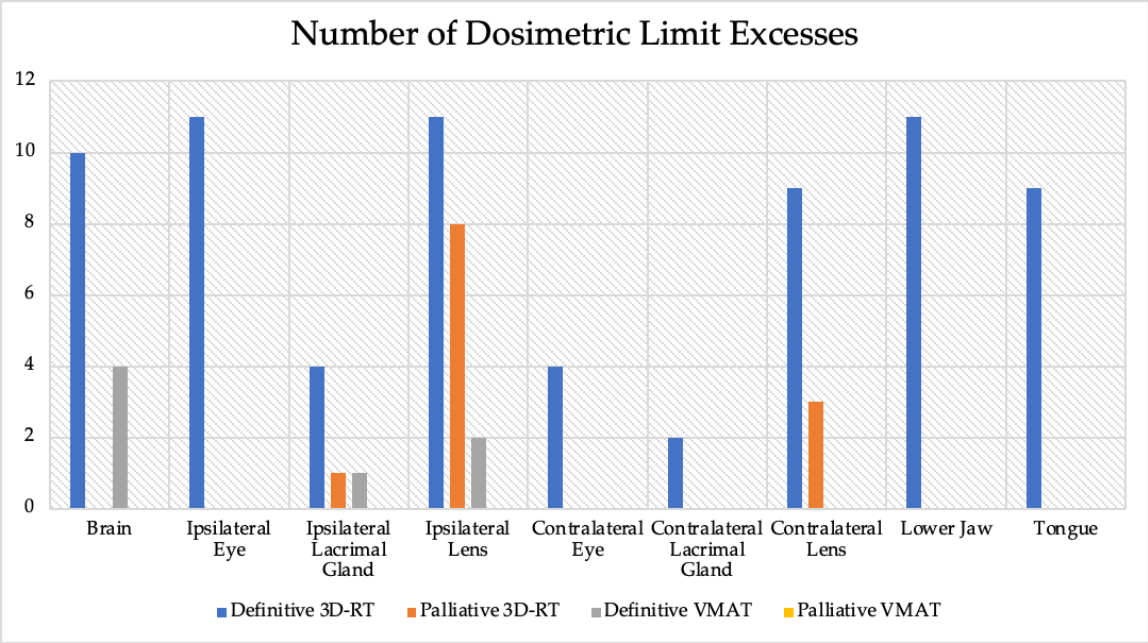

Fig. 30: Dosimetric limit excesses for the 3D-RT and VMAT plans.

For the definitive 3D-RT plans, the entire patient cohort exceeded the dosimetric limit for the ipsilateral eye, ipsilateral lens and the lower jaw. Also, tongue and the contralateral lens exceeded for most of the patients in definitive 3D-RT plans.

The dosimetric limits were achieved better for the palliative 3D-RT and VMAT plans, as the dose exposure was lower in general. In total, none of the palliative VMAT plans exceeded the dosimetric limit of any OAR.

As the VMAT delivery technique generates treatment fields more precisely, all OARs had a smaller number of dosimetric limit excesses compared to 3D-RT.

4.3 Comparison of the Results to the Literature

As the topic of this thesis is under ongoing research, only limited data was found in literature. Nevertheless, a 2021 study of "VMAT versus IMRT in canine stage 4 sinonasal tumors" by the Vetsuisse Faculty of the University of Zurich (UZH) achieved following delivered doses for OARs by the VMAT delivery technique for 10 dogs that differed in size, shape and breed: [53]

	UZH: Median [Gy]	**UZH: SA [Gy]**	**This Thesis: Median [Gy]**	**This Thesis: SA [Gy]**
PTV Prescribed dose by UZH: 42 Gy Prescribed dose in this thesis: 48 Gy	40,7	± 0,8	48,7	± 0,2
Eye_{higher} Dose constraint by UZH: 15 Gy Dose constraint in this thesis: 27 Gy	16,1	± 7,4	14,2	± 4,7
Eye_{lower} Dose constraint by UZH: 15 Gy Dose constraint in this thesis: 27 Gy	15,1	± 4,2	11,1	± 1,6
$Lacrimal\ gland_{higher}$ Dose constraint by UZH: 20 Gy Dose constraint in this thesis: 20 Gy	18,6	± 7,0	9,7	± 4,1
$Lacrimal\ gland_{lower}$ Dose constraint by UZH: 20 Gy Dose constraint in this thesis: 20 Gy	16,5	± 3,2	8,5	± 2,2

$Cornea_{higher}$ Dose constraint by UZH: 35,4 Gy Dose constraint in this thesis: 19 Gy	39,9	± 10,0	15,8	± 6,1
$Cornea_{lower}$ Dose constraint by UZH: 35,4 Gy Dose constraint in this thesis: 19 Gy	39,9	± 10,0	12,9	± 2,8
Brain Dose constraint by UZH: 26,4 Gy Dose constraint in this thesis: 47 Gy	36,9	± 6,2	41,3	± 12,4

T. 12: VMAT doses of OARs obtained by the University of Zurich for sinonasal tumors in dogs compared to this thesis' results. SA: Standard Abbreviation; Source: [53]

The most striking differences between this thesis and the study from the University of Zurich are [53]:

- Target coverages were chosen differently, however in the similar region except for the brain.
- The study of the University of Zurich was prescribing a dose of 42 Gy to the PTV, done in 10 fractions á 4,2 Gy.
- The treatment plan constraints in this thesis were lower for the lens/cornea, similar for the lacrimal gland and higher for the eye and brain.
- The achieved doses for the eyes were similar. The brain received a higher dose in this thesis and a lower for the lacrimal gland and the cornea/lens.

The University of Zurich concluded that VMAT plans were found to be superior in sparing OARs compared to IMRT. However, not all ocular OAR constraints

could be met while ensuring adequate dose coverage and restricting brain toxicity risk [53]. Hence, those results are overlapping with the results from this thesis.

VMAT delivery technique is part of modern radiotherapy in humans and used on all types of tumors. Multiple studies proved that compared to 3D-RT plans, VMAT plans provide a better dose homogeneity and highly conformal dose distributions while doses to OARs are reduced. Two comparable studies to this thesis include a 2012 study from the Department of Clinical Oncology of the Queen Elizabeth Hospital in Hong Kong and a study published in 2009 from the Department of Radiation Oncology of the University Medical Center Mannheim. In both studies, VMAT plans were compared to 3D-RT plans for humans. In the 2012 study in Hong Kong, 3D-RT and VMAT plans of advanced squamous cell cancer in the head and neck area were compared, whereas in the study in Mannheim compared 3D-RT and VMAT plans for prostate cancer. Those studies compared the doses that OARs like the heart, lungs, spinal cord or rectum received during treatment in 3D-RT and VMAT. Both concluded that a lower dose was delivered to the OARs by the VMAT plans, leading to a superiority of VMAT. Also, an extra finding in both studies was the reduced treatment time in VMAT plans. [54], [55] Therefore, the findings of both studies also overlap with the results from this thesis.

4.4 Limitations

The central limitations of the presented thesis arise from the low patient's number, no clinical data, in silico testing as well as limited experience of the planner, although continuously supervised.

First, the University of Veterinary Medicine Vienna provided data of 11 patients for this study. Since sinonasal tumors in dogs are not as common as other neoplasms, the amount of available data was therefore limited. The diversity of the patient cohort only give an excerpt of the challenges in veterinary oncology, as patients differ in tumor stage, size, breed and weight. Consequently, the results obtained are not able to make a reliable statement in general for this type of tumor and its treatment.

A further limitation arises from the theoretical nature of this thesis. A lack of supporting data for radiation therapy of sinonasal tumors in dogs was observed during research. Clinical trials are essential to investigate new therapy approaches in radiation oncology. As VMAT is established in human radiotherapy, it is rather new in veterinary oncology and consequently a lack of clinical data was found. However, the relevance of the VMAT treatment technique for animals in the future is evident and therefore subject of further research.

5 Conclusion and Outlook

The main task was to compare the doses the PTVs and the OARs received during 3D-RT and VMAT. Further tasks included the calculation of dosimetric limits for the dogs OARs and the measurement of the plans on a phantom with the Linac of the MUW/AKH.

The treatment plans developed in RayStation 11A revealed that the VMAT delivery technique achieved a significantly better target coverage as well as dose conformity and better results in terms of dose reduction for most of the surrounding OARs of the dogs' sinonasal tumors compared to 3D-RT. Although the superiority of VMAT was evident compared to 3D-RT for most of the OARs, a significant higher lower dose exposure was observed in the lacrimal gland.

Therefore, the main aim of this master's thesis to evaluate the impact of the improvements of modern radiation techniques in veterinary radiooncology could be met, proving that VMAT is a valuable technique for treatment in sinonasal tumors in dogs.

Based on this thesis, clinical implementation of VMAT will hopefully improve the clinical outcome for patients in the University of Veterinary Medicine Vienna in the future.

6 References

[1] L. Y. Pang and D. J. Argyle, "Veterinary oncology: Biology, big data and precision medicine," *Veterinary Journal*, vol. 213. Bailliere Tindall Ltd, pp. 38–45, Jul. 01, 2016. doi: 10.1016/j.tvjl.2016.03.009.

[2] M. Teoh, C. H. Clark, K. Wood, S. Whitaker, and A. Nisbet, "Volumetric modulated arc therapy: A review of current literature and clinical use in practice," *British Journal of Radiology*, vol. 84, no. 1007. pp. 967–996, Nov. 2011. doi: 10.1259/bjr/22373346.

[3] G. C. Pereira, M. Traughber, and R. F. Muzic, "The role of imaging in radiation therapy planning: Past, present, and future," *BioMed Research International*, vol. 2014. Hindawi Publishing Corporation, 2014. doi: 10.1155/2014/231090.

[4] H. L. Gardner, J. M. Fenger, and C. A. London, "Dogs as a model for cancer," *Annual Review of Animal Biosciences*, vol. 4. Annual Reviews Inc., pp. 199–222, Feb. 15, 2016. doi: 10.1146/annurev-animal-022114-110911.

[5] FEDIAF and Emma Bedford, "Number of pet dogs in Austria from 2010 to 2020 (in 1000s)," *https://www.statista.com/statistics/515489/dog-population-europe-austria/*, Jun. 2021.

[6] J. L. Kelsey, A. S. Moore, and L. T. Glickman, "Epidemiologic Studies of Risk Factors for Cancer in Pet Dogs," 1998. [Online]. Available: https://academic.oup.com/epirev/article/20/2/204/435975

[7] H. I. Kim, H. Lim, and A. Moon, "Sex differences in cancer: Epidemiology, genetics and therapy," *Biomolecules and Therapeutics*, vol. 26, no. 4. Korean Society of Applied Pharmacology, pp. 335–342, Jul. 01, 2018. doi: 10.4062/biomolther.2018.103.

[8] M. Staff, "Cancer Treatment," May 2020.

[9] PennVet, "Management of Radiation Side Effects." https://www.vet.upenn.edu/docs/default-source/ryan/comprehensive-cancer-care/radiation-oncology/management-of-radiation-side-effects.pdf?sfvrsn=2745eeba_0 (accessed May 03, 2022).

[10] S. R. Mehta, V. Suhag, M. Semwal, and N. Sharma, "Radiotherapy: Basic concepts and recent advances," *Medical Journal Armed Forces India*, vol. 66,

no. 2. Medical Journal Armed Forces India, pp. 158–162, 2010. doi: 10.1016/S0377-1237(10)80132-7.

[11] "2-2 RSSC FUNDAMENTAL RADIATION CONCEPTS."

[12] D. R. Dance, S. Christofides, A. D. A. Maidment, I. D. Mclean, and K. H. Ng, *Diagnostic Radiology Physics: A Handbook for Teachers and Students*. Vienna: IAEA, 2014.

[13] *Radiation Biology: A Handbook for Teachers and Students*. Vienna: International Atomic Energy Agency, 2010.

[14] M. Alenezi and M. Maqbool, "KLEIN-NISHINA ELECTRONIC CROSS SECTION, COMPTON SCATTERING CROSS SECTION, LINEAR ATTENUATION COEFFIECIENT AND BUILD UP FACTOR OF WAX FOR RADIATION PROTECTIO AND SAFETY A RESEARCH PROJECT SUBMITTED TO THE GRADUATE SCHOOL IN PARTIAL FULFILLMENT OF THE REQUIREMENTS FOR THE DEGREE MASTER OF ART," 2017.

[15] E. B. Podgorsak, "Radiation Oncology Physics: A Handbook for Teachers and Students."

[16] E. B. Podgorsak, "Radiation Oncology Physics: A Handbook for Teachers and Students."

[17] D. Georg, T. Knöös, and B. McClean, "Current status and future perspective of flattening filter free photon beams," *Medical Physics*, vol. 38, no. 3, pp. 1280–1293, 2011, doi: 10.1118/1.3554643.

[18] J. M. Galvin, A. R. Smith, and B. Lally, *Characterization of a multileaf collimator system*, 2nd ed., vol. 25. 1993.

[19] M. S. Huq, I. J. Das, T. Steinberg, and J. M. Galvin, "A dosimetric comparison of various multileaf collimators," *Physics in Medicine and Biology*, vol. 47, no. 12, pp. N159–N170, Jun. 2002, doi: 10.1088/0031-9155/47/12/401.

[20] J. M. Galvin, "THE MULTILEAF COLLIMATOR-A COMPLETE GUIDE."

[21] J. Deng, T. Pawlicki, Y. Chen, J. S. Li, S. B. Jiang, and C. M. Ma, "The MLC tongue-and-groove effect on IMRT dose distributions," in *Annual International Conference of the IEEE Engineering in Medicine and Biology - Proceedings*, 2000, vol. 3, pp. 2075–2078. doi: 10.1109/iembs.2000.900534.

[22] P. Mayles, A. Nahum, and J. C. Rosenwald, *Handbook of Radiotherapy Physics: Theory and Practice*, 1st ed. Boca Raton: CRC Press, 2007.

[23] S. H. Choi and J. Seong, "Strategic application of radiotherapy for hepatocellular carcinoma," *Clinical and Molecular Hepatology*, vol. 24, no. 2. Korean Association for the Study of the Liver, pp. 114–134, Jun. 01, 2018. doi: 10.3350/cmh.2017.0073.

[24] K. Y. Cheung, "Intensity modulated radiotherapy: Advantages, limitations and future developments," *Biomedical Imaging and Intervention Journal*, vol. 2, no. 1. 2006. doi: 10.2349/biij.2.1.e19.

[25] T. Y. Chan, P. W. Tan, and J. I. Tang, "Intensity-modulated radiation therapy for early-stage breast cancer: Is it ready for prime time?," *Breast Cancer: Targets and Therapy*, vol. 9. Dove Medical Press Ltd., pp. 177–183, Mar. 20, 2017. doi: 10.2147/BCTT.S127583.

[26] N. Hodapp, "Der ICRU-Report 83: Verordnung, Dokumentation und Kommunikation der fluenzmodulierten Photonenstrahlentherapie (IMRT)," *Strahlentherapie und Onkologie*, pp. 97–100, Jan. 2012.

[27] C. Khamphan, J. Balosso, A. Chaikh, T. Kumar, and R. Garcia, "What should we know about photon dose calculation algorithms used for radiotherapy? Their impact on dose distribution and medical decisions based on TCP/NTCP," *Oncol*, vol. 4, no. 4, 2016, doi: 10.14319/ijcto.44.18.

[28] N. G. Burnet, S. J. Thomas, K. E. Burton, and S. J. Jefferies, "Defining the tumour and target volumes for radiotherapy," *Cancer Imaging*, vol. 4, no. 2, pp. 153–161, 2004, doi: 10.1102/1470-7330.2004.0054.

[29] A. K. Berthelsen *et al.*, "What's new in target volume definition for radiologists in ICRU Report 71? How can the ICRU volume definitions be integrated in clinical practice?," *Cancer Imaging*, vol. 7, no. 1. pp. 104–116, 2007. doi: 10.1102/1470-7330.2007.0013.

[30] I. l R. J A Antolak, "Planning target volumes for radiotherapy: how much margin is needed?," The University of Texas M. D. Anderson Cancer Center, Houston, Texas, USA, 1999.

[31] Z. Jafry, A. Gal, A. Fleck, J. Darko, and V. J. Poirier, "Proposed expansion margins for planning organ at risk volume for lenses during radiation therapy of the nasal cavity in dogs and cats," *Veterinary Radiology and Ultrasound*, vol. 58, no. 4, pp. 471–478, Jul. 2017, doi: 10.1111/vru.12490.

[32] Z. Shen *et al.*, "Correlation between the γ passing rates of IMRT plans and the volumes of air cavities and bony structures in head and neck cancer," *Radiation Oncology*, vol. 16, no. 1, Dec. 2021, doi: 10.1186/s13014-021-01861-y.

[33] M. Hussein, C. H. Clark, and A. Nisbet, "Challenges in calculation of the gamma index in radiotherapy – Towards good practice," *Physica Medica*, vol. 36, pp. 1–11, 2017, doi: https://doi.org/10.1016/j.ejmp.2017.03.001.

[34] T. Ju, T. Simpson, J. O. Deasy, and D. A. Low, "Geometric interpretation of the γ dose distribution comparison technique: Interpolation-free calculation," *Medical Physics*, vol. 35, no. 3, pp. 879–887, 2008, doi: 10.1118/1.2836952.

[35] S. Webb, "The physical basis of IMRT and inverse planning," *British Journal of Radiology*, vol. 76, no. 910. pp. 678–689, Oct. 2003. doi: 10.1259/bjr/65676879.

[36] M. Kara Bucci, A. Bevan, and M. I. Roach, "Advances in Radiation Therapy Conventional to 3D, to IMRT, to 4D and Beyond," *2*, vol. 55, pp. 117–133, Apr. 2005.

[37] A. Taylor and M. E. B. Powell, "Intensity-modulated radiotherapy - What is it?," *Cancer Imaging*, vol. 4, no. 2, pp. 68–73, 2004, doi: 10.1102/1470-7330.2004.0003.

[38] J. L. Bedford, "Treatment planning for volumetric modulated arc therapy," *Medical Physics*, vol. 36, no. 11, pp. 5128–5138, 2009, doi: 10.1118/1.3240488.

[39] D. Meuten, Ed., *Tumors in Domestic Animals*, 5th ed. Raleigh, NC: John Wiley & Sons, Inc., 2017. Accessed: May 03, 2022. [Online]. Available: https://onlinelibrary.wiley.com/doi/pdf/10.1002/9781119181200

[40] K. M. Elliot and M. N. Mayer, "Oncology Corner Le coin de l'oncologie Radiation therapy for tumors of the nasal cavity and paranasal sinuses in dogs." Accessed: Mar. 29, 2022. [Online]. Available: https://www.ncbi.nlm.nih.gov/pmc/articles/PMC2643460/

[41] A. Patel, "Benign vs Malignant Tumors," *JAMA Oncology*, vol. 6, no. 9, p. 1488, Sep. 2020, doi: 10.1001/jamaoncol.2020.2592.

[42] J. W. Potter, K. B. Jones, and J. J. Barrott, "Sarcoma–The standard-bearer in cancer discovery," *Critical Reviews in Oncology/Hematology*, vol. 126. Elsevier Ireland Ltd, pp. 1–5, Jun. 01, 2018. doi: 10.1016/j.critrevonc.2018.03.007.

[43] R. A. Weinberg, *The Biology of Cancer*, 2nd ed., vol. 1. New York: W.W. Norton & Company, 2013.

[44] V. J. Poirier, E. S. Y. Koh, J. Darko, A. Fleck, C. Pinard, and D. M. Vail, "Patterns of local residual disease and local failure after intensity modulated/image guided radiation therapy for sinonasal tumors in dogs," *Journal of Veterinary Internal Medicine*, vol. 35, no. 2, pp. 1062–1072, Mar. 2021, doi: 10.1111/jvim.16076.

[45] "What are the Goals of Radiation Therapy?," Dec. 2012. https://d34y695x0pxlvj.cloudfront.net/wp-content/uploads/2016/12/What-are-the-goals-of-radiation-therapy.pdf (accessed May 03, 2022).

[46] Y. Matsuya, K. Tsutsumi, K. Sasaki, and H. Date, "Evaluation of the cell survival curve under radiation exposure based on the kinetics of lesions in relation to dose-delivery time," *Journal of Radiation Research*, vol. 56, no. 1, pp. 90–99, May 2014, doi: 10.1093/jrr/rru090.

[47] N. S. Hegemann, M. Guckenberger, C. Belka, U. Ganswindt, F. Manapov, and M. Li, "Hypofractionated radiotherapy for prostate cancer," *Radiation Oncology*, vol. 9, no. 1. BioMed Central Ltd., Dec. 06, 2014. doi: 10.1186/s13014-014-0275-6.

[48] "Elekta Infinity."

[49] "ELEKTA Infinity catalogue."

[50] C. Voyant, D. Julian, R. Roustit, K. Biffi, and C. Lantieri, "Biological effects and equivalent doses in radiotherapy: A software solution," *Reports of Practical Oncology and Radiotherapy*, vol. 19, no. 1, pp. 47–55, 2014, doi: 10.1016/j.rpor.2013.08.004.

[51] R. Shier, "Statistics: 1.1 Paired t-tests," Loughborough, 2004. Accessed: May 04, 2022. [Online]. Available: https://www.lboro.ac.uk/departments/mlsc/student-resources/statistics-leaflets/

[52] H. Li, L. Dong, L. Zhang, J. N. Yang, M. T. Gillin, and X. R. Zhu, "Toward a better understanding of the gamma index: Investigation of parameters with a surface-based distance method," *Medical Physics*, vol. 38, no. 12, pp. 6730–6741, 2011, doi: 10.1118/1.3659707.

[53] V. Meier, F. Czichon, L. Walsh, and C. R. Bley, "Can volumetric modulated arc radiation therapy reduce organ at risk dose in stage 4 sinonasal tumors in dogs treated with boost irradiation?," *PLoS ONE*, vol. 16, no. 10 October, Oct. 2021, doi: 10.1371/journal.pone.0259112.

[54] S. Lee, C. Lee, K. Yu, and K. Ngan, "Volumetric Modulated Arc Therapy vs 3-Dimensional Conformal Radiotherapy in Head and Neck Cancer: a Comparative Planning and Dosimetry Study," 2012.

[55] D. Wolff *et al.*, "Volumetric modulated arc therapy (VMAT) vs. serial tomotherapy, step-and-shoot IMRT and 3D-conformal RT for treatment of prostate cancer," *Radiotherapy and Oncology*, vol. 93, no. 2, pp. 226–233, Nov. 2009, doi: 10.1016/j.radonc.2009.08.011.

7 Erklärung

Hiermit erkläre ich, dass ich die vorliegende Arbeit in allen Teilen selbstständig und nur unter Zuhilfenahme der angegebenen Quellen und Literatur verfasst habe.

Wien, den 28.07.2022

_____

David Steinberger

8 Appendix

8.1 Organs At Risk

8.1.1 Ipsilateral Eye

	a) Definitive Plans		b) Palliative Plans	
	3D-RT [Gy]	**VMAT [Gy]**	**3D-RT [Gy]**	**VMAT [Gy]**
Mean	40,8	14,2	17,0	9,5
Standard Deviation	8,0	4,8	3,4	1,3
Max	49,5	24,7	20,3	11,5
Min	26,5	9,5	10,5	7,3
IQR: Q1	35,3	10,7	15,0	8,7
IQR: Q3	47,7	14,9	19,8	10,3
P-Value	2,11665E-07		1,6517E-06	
Alpha	0,05		0,05	
Hypothesis	H_1		H_1	

T. 13: Dose-values of the ipsilateral eye in definitive and palliative 3D-RT- and VMAT-plans.

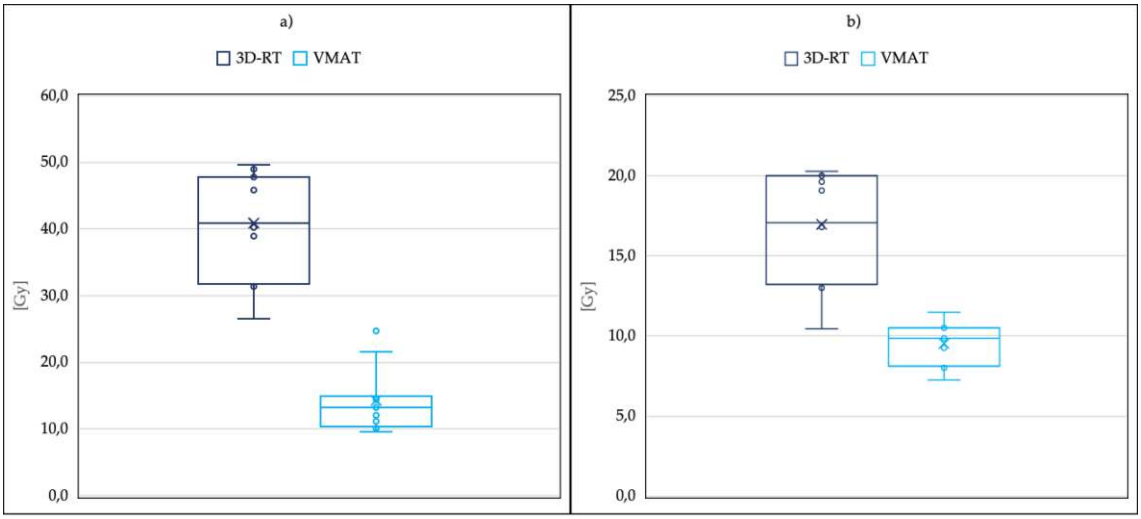

Fig. 31: Box-plots of 3D-RT and VMAT Gy-values of the ipsilateral eye: a) Definitive plans, b) Palliative plans.

8.1.2 Ipsilateral Lacrimal Gland

	a) Definitive Plans		b) Palliative Plans	
	3D-RT [Gy]	**VMAT [Gy]**	**3D-RT [Gy]**	**VMAT [Gy]**
	19,5	9,6	8,2	5,3
Mean	19,2	4,4	8,1	1,2
Standard Deviation	48,0	21,6	20,9	7,2
Max	2,0	4,5	0,8	2,7
Min	3,9	7,7	1,6	4,8
IQR: Q1	41,2	10,0	16,9	5,9
IQR: Q3	0,123104006		0,20936326	
P-Value	0,05		0,05	
Alpha	H_0		H_0	

T. 14: Dose-values of the ipsilateral lacrimal gland in definitive and palliative 3D-RT- and VMAT-plans.

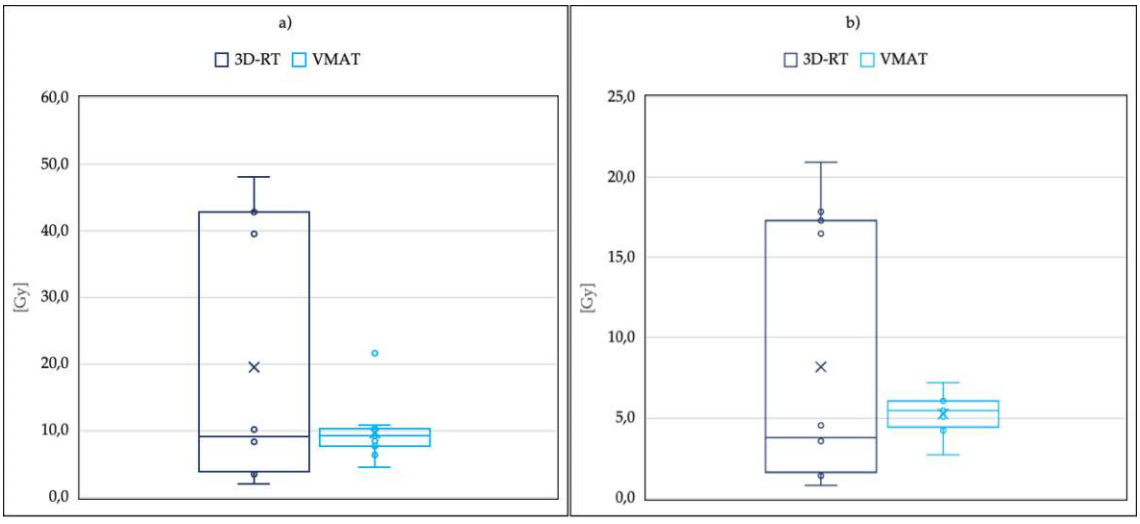

Fig. 32: Box-plots of 3D-RT and VMAT Gy-values of the ipsilateral lacrimal gland: a) Definitive plans, b) Palliative plans.

8.1.3 Ipsilateral Lens

	a) Definitive Plans		b) Palliative Plans	
	3D-RT [Gy]	**VMAT [Gy]**	**3D-RT [Gy]**	**VMAT [Gy]**
Mean	46,0	15,9	18,8	11,7
Standard Deviation	4,6	6,4	2,2	2,6
Max	50,4	30,1	20,8	15,0
Min	33,1	9,6	13,8	5,6
IQR: Q1	46,1	11,7	18,3	11,2
IQR: Q3	48,1	16,5	20,2	13,3
P-Value	2,08616E-08		3,2374E-07	
Alpha	0,05		0,05	
Hypothesis	H_1		H_1	

T. 15: Dose-values of the ipsilateral lens in definitive and palliative 3D-RT- and VMAT-plans.

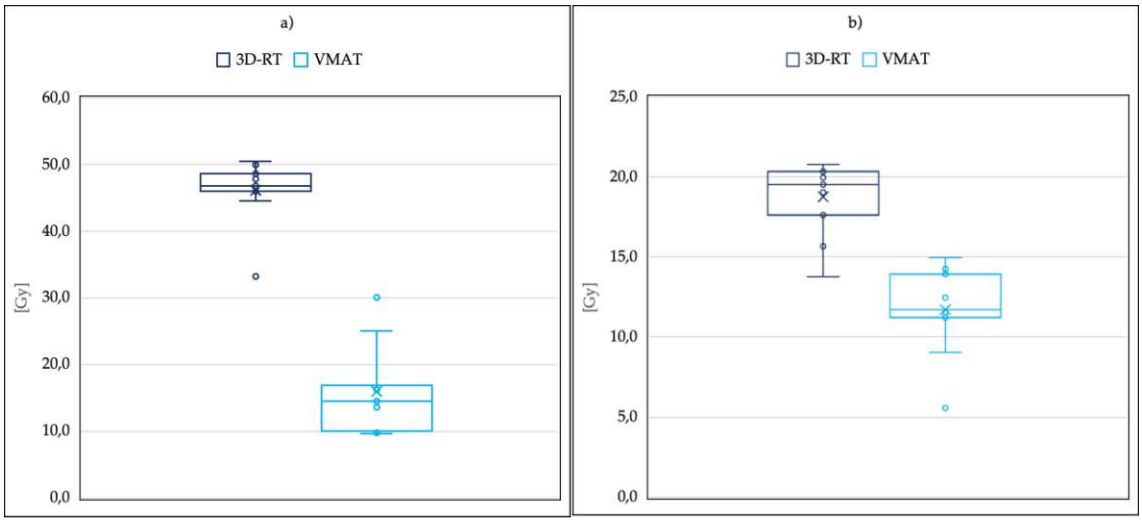

Fig. 33: Box-plots of 3D-RT and VMAT Gy-values of the ipsilateral lens: a) Definitive plans, b) Palliative plans.

8.1.4 Contralateral Eye

	a) Definitive Plans		b) Palliative Plans	
	3D-RT [Gy]	**VMAT [Gy]**	**3D-RT [Gy]**	**VMAT [Gy]**
Mean	20,1	11,1	8,4	9,0
Standard Deviation	8,4	1,7	3,5	1,8
Max	31,9	13,7	13,1	11,3
Min	2,9	8,5	1,1	5,3
IQR: Q1	15,6	9,7	6,6	8,1
IQR: Q3	26,7	12,4	11,1	10,3
P-Value	0,003672117		0,57944892	
Alpha	0,05		0,05	
Hypothesis	H_1		H_0	

T. 16: Dose-values of the contralateral eye in definitive and palliative 3D-RT- and VMAT-plans.

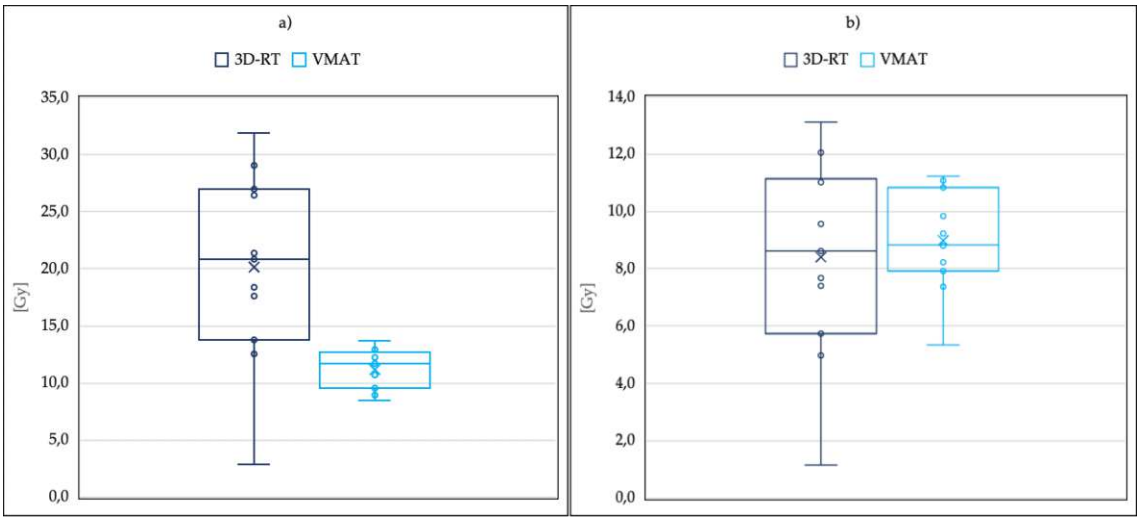

Fig. 34: Box-plots of 3D-RT and VMAT Gy-values of the contralateral eye: a) Definitive plans, b) Palliative plans.

8.1.5 Contralateral Lens

	a) Definitive Plans		b) Palliative Plans	
	3D-RT [Gy]	**VMAT [Gy]**	**3D-RT [Gy]**	**VMAT [Gy]**
Mean	31,5	12,9	12,1	11,7
Standard Deviation	13,1	2,9	6,3	3,0
Max	46,3	17,9	19,0	15,5
Min	3,3	8,8	1,3	7,3
IQR: Q1	26,7	11,1	8,3	8,9
IQR: Q3	40,8	14,9	17,3	14,0
P-Value	0,001782623		0,81814089	
Alpha	0,05		0,05	
Hypothesis	H_1		H_0	

T. 17: Dose-values of the contralateral lens in definitive and palliative 3D-RT- and VMAT-plans.

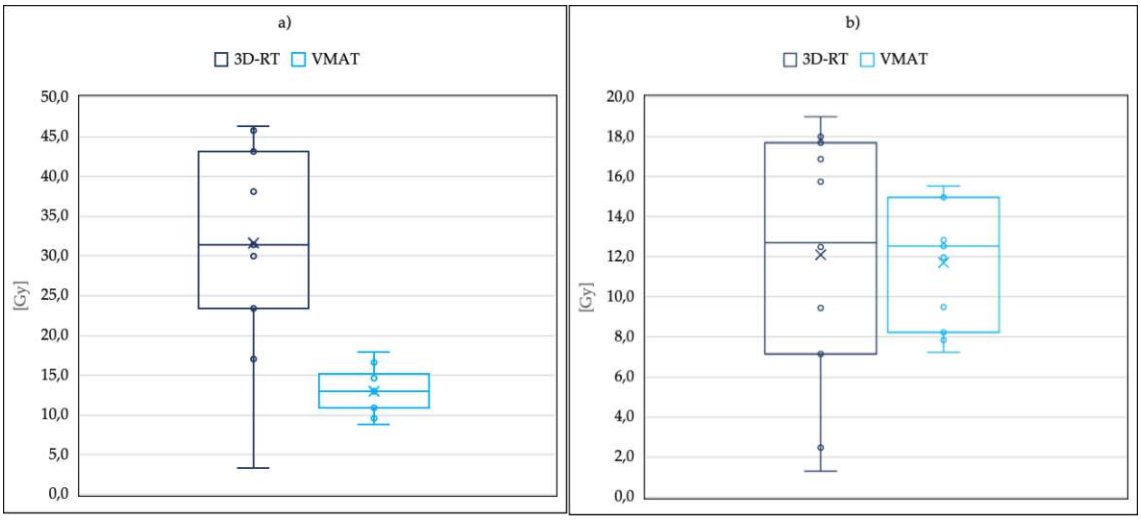

Fig. 35: Box-plots of 3D-RT and VMAT Gy-values of the contralateral lens: a) Definitive plans, b) Palliative plans.